


Distinct Life Histories Impact Dikaryotic Genome Evolution in the Rust Fungus *Puccinia striiformis* Causing Stripe Rust in Wheat

Benjamin Schwessinger ^{1,*†}, Yan-Jun Chen^{2,†}, Richard Tien³, Josef Korbinian Vogt⁴, Jana Sperschneider⁵, Ramawatar Nagar¹, Mark McMullan⁶, Thomas Sicheritz-Ponten², Chris K. Sørensen⁷, Mogens Støvring Hovmøller⁷, John P. Rathjen^{1,*}, and Annemarie Fejer Justesen^{7,*}

¹Research School of Biology, The Australian National University, Acton, Canberra, Australian Capital Territory, Australia

²The GLOBE Institute, Faculty of Health and Medical Sciences, University of Copenhagen, Denmark

³School of Dentistry, The University of Western Australia, Nedlands, Western Australia, Australia

⁴Novo Nordisk Foundation Center for Basic Metabolic Research, University of Copenhagen, Denmark

⁵Biological Data Science Institute, The Australian National University, Acton, Canberra, Australian Capital Territory, Australia

⁶Earlham Institute, Norwich Research Park, United Kingdom

⁷Department of Agroecology, Faculty of Science and Technology, Aarhus University, Slagelse, Denmark

[†]These authors contributed equally to this work.

*Corresponding authors: E-mails: benjamin.schwessinger@anu.edu.au; john.rathjen@anu.edu.au; annemariefejer.justesen@agro.au.dk.

Accepted: April 3, 2020

Data deposition: This project has been deposited at NCBI under the accessions SAMN12098061, PRJNA588102, WXXWY00000000, WXXW00000000, and MN746374. This project has been deposited at zenodo under the accession 10.5281/zenodo.3556840, 10.5281/zenodo.3663113, 10.5281/zenodo.3663111, and 10.5281/zenodo.3663116. This project has been deposited at github under the accession https://github.com/Team-Schwessinger/DK_0911-1.

Abstract

Stripe rust of wheat, caused by the obligate biotrophic fungus *Puccinia striiformis* f.sp. *tritici*, is a major threat to wheat production worldwide with an estimated yearly loss of US \$1 billion. The recent advances in long-read sequencing technologies and tailored-assembly algorithms enabled us to disentangle the two haploid genomes of *Pst*. This provides us with haplotype-specific information at a whole-genome level. Exploiting this novel information, we perform whole-genome comparative genomics of two *P. striiformis* f.sp. *tritici* isolates with contrasting life histories. We compare one isolate of the old European lineage (PstS0), which has been asexual for over 50 years, and a Warrior isolate (PstS7 lineage) from a novel incursion into Europe in 2011 from a sexual population in the Himalayan region. This comparison provides evidence that long-term asexual evolution leads to genome expansion, accumulation of transposable elements, and increased heterozygosity at the single nucleotide, structural, and allele levels. At the whole-genome level, candidate effectors are not compartmentalized and do not exhibit reduced levels of synteny. Yet we were able to identify two subsets of candidate effector populations. About 70% of candidate effectors are invariant between the two isolates, whereas 30% are hypervariable. The latter might be involved in host adaptation on wheat and explain the different phenotypes of the two isolates. Overall, this detailed comparative analysis of two haplotype-aware assemblies of *P. striiformis* f.sp. *tritici* is the first step in understanding the evolution of dikaryotic rust fungi at a whole-genome level.

Key words: Basidiomycetes, dikaryon, haplotype, plant pathogen, asexual reproduction, sexual reproduction, wheat yellow rust, wheat stripe rust.

Introduction

Fungi have complex life cycles involving clonal as well as sexual reproduction. Sex in fungi is often associated with dispersal, dormancy, and survival under adverse conditions such as the absence of hosts (Anikster 1986). Sexual reproduction creates genotypic diversity and enables adaptation to new environments by combining beneficial alleles and eliminating harmful genetic traits (Heitman 2015; Seudre et al. 2018). The advantage of asexual reproduction, on the other hand, is the rapid multiplication and spread of the most well-adapted individuals. In some species, sexual reproduction is so rare or cryptic that the sexual cycle historically was thought to be absent and only recently has been discovered (Zeyl 2009; Taylor et al. 2015). Studies of the genomic architecture of fungal pathogens with different reproduction strategies can help us to understand the genetic and genomic processes behind pathogen adaptation. This knowledge is important for predicting the response of pathogens to challenges such as climate change, drugs, fungicides, host resistance, or immunity, and will strengthen the development of methods for combating fungal pathogens (Gladieux et al. 2014).

Rust fungi, the *Pucciniales*, are a large group of fungal plant pathogens, some of which impact severely on agricultural and forest production (Lorrain et al. 2019). They depend on living host cells and have complex life cycles, which may comprise many spore types over two phylogenetically distinct host plants for completion of the sexual life cycle. *Puccinia striiformis* causes yellow (stripe) rust on cereals and grasses and has historically been restricted to temperate-cool and wet climates (Rapilly 1979). Since 2000, new aggressive strains adapted to higher temperatures have caused the expansion of the disease into warmer regions, and it is currently one of the most prevalent and damaging diseases on common wheat (*Triticum aestivum* L.) worldwide (Wellings 2011; Beddow et al. 2015; Singh et al. 2016; Savary et al. 2019). During the asexual life cycle, which recurs several times during the wheat growing season, *P. striiformis* produces dikaryotic urediniospores which reinfect wheat (Schwessinger 2017). These spores are wind borne and may spread over long distances to introduce exotic strains into new areas (Hovmøller et al. 2016). Historically, the sexual cycle of *P. striiformis* has been a great mystery and many years of search for the alternate host were fruitless until it was shown that barberry (*Berberis* spp.) can serve as the alternate host for completion of the sexual cycle (Jin et al. 2010). The significance of *Berberis* spp. as an alternate host for *P. striiformis* in nature is still unknown, but high levels of genetic diversity in *P. striiformis* populations in China and Pakistan indicate that sexual reproduction is taking place under natural conditions, and the near-Himalayan region is the likely center of genetic diversity for *P. striiformis* (Duan et al. 2010; Mboup et al. 2012; Ali et al. 2014, 2016). In contrast, reproduction of *P. striiformis* in Europe, United States, and Australia is clonal, and adaptation

to host resistance happens through stepwise mutations (Steele et al. 2001; Hovmøller and Justesen 2007; Markell and Milus 2008; Chen et al. 2014). These mutations lead to the loss of recognition of *P. striiformis* effectors which previously were recognized by specific plant resistance (*R*) gene products and *P. striiformis* is then termed virulent to the specific *R* gene. In the absence of recognition, for example, in a wheat plant that lacks the corresponding *R* gene, effectors suppress plant immune responses and facilitate the infection process (Ellis et al. 2014).

Only few clonal lineages of *P. striiformis* are responsible for the yellow rust epidemics worldwide, and stepwise mutation and clonal reproduction has been the major driving force for the evolution of new virulent races that can overcome widely deployed resistance genes (Hovmøller et al. 2008; Walter et al. 2016; Ali et al. 2017). Combination of virulence alleles by sexual or somatic recombination may also generate strains with new virulence profiles, the later was recently demonstrated for the *Puccinia graminis* f.sp. *tritici* isolate Ug99 (Li, Upadhyaya, et al. 2019). The exact frequency of these mechanisms in nature is not yet known, but it may be more common than previously anticipated (Li, Upadhyaya, et al. 2019). Based on observational studies of >2,000 alive isolates representing worldwide collections of *P. striiformis*, we have noted that isolates linked to long-term asexual lineages generally produce fewer teliospores compared with isolates from areas with sexual populations, and compared with first generation progeny isolates raised from sexual reproduction on *Berberis vulgaris* in particular (Rodriguez-Algaba et al. 2014). This observation is supported by Ali et al. (2014), where isolates from China, Pakistan, and Nepal, which is considered center of genetic diversity for *P. striiformis*, produced more telia than isolates from, for example, Europe (Ali et al. 2010, 2014). Teliospores are obligatory for completing the sexual life cycle and this indicates that these long-term clonal lineages may have a reduced ability to undergo sexual reproduction (Ali et al. 2010).

In 2011, a new *P. striiformis* lineage, PstS7, known generally as Warrior was detected in high frequency on both wheat and triticale (*x Triticosecale*) in many European countries (Hubbard et al. 2015; Hovmøller et al. 2016). It was able to cause disease on cultivated host varieties that had previously been resistant (Sørensen et al. 2014). Moreover, it produced high amounts of teliospores and was able to complete the sexual cycle on barberry under experimental conditions (Rodriguez-Algaba et al. 2014). Warrior is genetically very different from the clonal lineages present in Europe before 2011 (e.g., PstS0) and similar to isolates originating from the center of diversity in the near-Himalayan region (Hubbard et al. 2015; Hovmøller et al. 2016). Determining the mechanisms behind the generation of new virulent strains of *P. striiformis* such as Warrior is important. However, sequencing technologies available to date have provided only limited understanding of genetic recombination, comprising somatic,

parasexual, and sexual recombination, as a driving force for generating new strains of the pathogen.

Until recently, most draft genome assemblies of *P. striiformis* were based largely on short-read sequencing data (Cantu et al. 2011, 2013; Zheng et al. 2013). However, short-read sequencing data are not well suited to the dikaryotic rusts due to the high proportion of repetitive sequences (>50%), high heterozygosity, leading to the difficulty in phasing and high level of fragmentation of the two haploid genomes. Hence, short-read assemblies typically lack contiguity and individual haplotype information. Single molecule-sequencing technologies such as PacBio and Nanopore produce far longer reads, which in combination with novel assembly algorithms have provided more accurate (Xia et al. 2018) and complete genomes with effective haplotype phasing (Schwessinger et al. 2018). Here, we provide a genome assembly of a Warrior isolate sampled in Denmark (Pst-DK0911) using long-read sequencing and a diploid-aware genome assembler (Chin et al. 2016; Schwessinger et al. 2018). We previously produced a highly phased and contiguous assembly of Pst-104E (Schwessinger et al. 2018), an Australian isolate, which represents the first pathotype of *P. striiformis* detected in Australia in 1979 (Wellings and McIntosh 1990). This isolate is almost identical to European isolates belonging to the PstS0 lineage with respect to virulence and genotype (Steele et al. 2001; Hovmøller et al. 2008; Thach et al. 2016). The PstS0 lineage is strictly clonal (Hovmøller et al. 2002) and evolution of new races by step-wise mutations can be traced back to at least 1950s (Hovmøller and Justesen 2007; Thach et al. 2016). Isolates of the PstS0 lineage produce less teliospores with reduced ability to germinate and to complete the sexual life cycle on *Berberis* spp. (Ali et al. 2010).

This new genome assembly allows whole-genome comparisons between two isolates representing contrasting lifestyles of *P. striiformis*. It provides detailed insights into the adaptive divergence and evolution of *P. striiformis* and rust fungi in general. Specifically, we explore questions around the impact of sexual and asexual reproduction on structural genomic evolution, the generation of genetic diversity, and host adaptation.

Materials and Methods

Puccinia striiformis f.sp. *tritici* Pathotype, Growth Conditions, and Spore Amplification

The Pst-DK0911 isolate was purified from a single lesion sampled from the commercial wheat cv. Holeby in Denmark in 2011. The isolate was race phenotyped according to Hovmøller et al. (2016) and genotyped as described previously (Rodriguez-Algaba et al. 2014; Hovmøller et al. 2016). The Pst-104E is an isolate of the pathotype 104E137A- and was collected from the field in 1982 (Plant Breeding Institute

accession number 821559 = 415). The sequencing and analysis of this isolate were described previously (Wellings 2007; Schwessinger et al. 2018). The same isolate ID was used in the study of Hovmøller et al. (2008), confirming the immediate connection between the old NW-European population and the Australian *P. striiformis* population up to 2001. The Pst-DK0911 isolate was multiplied on susceptible seedlings of wheat cv. Morocco, which were inoculated using the method described (Sørensen et al. 2016). The inoculated seedlings were misted with water and incubated at 10 °C in the dark for 24 h and 100% relative humidity (dew formation) in an incubation room. After incubation, the inoculated plants were transferred to quarantine spore-proof greenhouse cabinets with a temperature regime of 17 °C day and 12 °C night, and a light regime of 16 h photoperiod of natural light and supplemental sodium light (100 $\mu\text{mol/s/m}^2$), and 8 h dark. The plants were covered with cellophane bags 5–7 days after infection (dai) to avoid cross-contamination before sporulation. The urediniospores were harvested at 15–20 dai and freeze-dried before DNA extraction.

DNA Extraction and Genome Sequencing

We extracted DNA from freeze-dried urediniospores as described previously (Schwessinger and Rathjen 2017) with few modifications. A volume of 875 μl lysis buffer was used per 60 mg spores in a 2-ml eppendorf tube. Library preparation and PacBio sequencing were performed at the Earlham Institute (Norwich, United Kingdom). One DNA library was sequenced on a PacBio RSII instrument using P6-C4 chemistry and 16 SMRT cells were sequenced in total. Moreover, a DNA sample from the same isolate was sequenced using Illumina short-read technology. A TruSeq library was sequenced on a HiSeq 2000 instrument as a 100 bases paired-end library at the Danish National High-Throughput DNA Sequencing Centre (Copenhagen, Denmark).

RNAseq

Pst-DK0911 was point inoculated on leaves of the susceptible cv. Avocet S with a pipette using 5 μl spore suspension in 3 M Novex 7100 (2 mg spores per ml) as described previously (Sørensen et al. 2016) without fixation of leaves. Three replicates were prepared and leaf segments of 10–12 mm of the second leaves of each replicate were harvested at 7 and 9 dai for transcriptome sequencing. We isolated total RNAs with the RNeasy Plant Mini kit (Qiagen) from 100 mg of infected leaf tissues including a DNaseI (Qiagen) treatment according to the manufacturer's instructions. Transcriptome libraries were generated using the TruSeq Stranded Total RNA with Ribo-Zero plant kit (Illumina) according to the standard protocol to remove cytoplasmic, mitochondrial, and chloroplast ribosomal RNA. Next-generation sequencing for six multiplexed samples was performed using an Illumina HiSeq 2000 sequencer at BGI (Copenhagen, Denmark).

Genome Assembly

For genome assembly, we used FALCON and FALCON-Unzip (Chin et al. 2016) github tag 1.7.4 with the parameters described in [supplementary data 1](#) and [2](#), [Supplementary Material](#) online. We checked the resulting contigs for eukaryotic and prokaryotic contamination by BlastN searches against the NCBI nucleotide reference database (downloaded 04052016) (Altschul et al. 1990). None of the contigs showed signs of contamination as estimated via best BLAST hits at a given position. We performed two manual curation steps. In the first step, we reasoned that some of the primary contigs without corresponding haplotigs might actually represent haplotigs that could not be assigned to their respective primary contigs in the assembly graph because of too large a difference between the two haplotypes. We aligned all primary contigs without haplotigs to primary contigs with haplotigs using MUMmer version 3 (Kurtz et al. 2004). We screened the best alignments of each primary contig without haplotig for percentage alignment, length of alignment, and if they aligned to regions in the primary contigs that previously had not been covered by a haplotig alignment. Using this approach, we reassigned five primary contigs without haplotigs (~6 Mb) to haplotigs.

Repeat Annotation and Analysis

Repeat regions were annotated as described previously (Schwessinger et al. 2018) using the REPET pipeline v2.5 (Quesneville et al. 2005; Flutre et al. 2011; Maumus and Quesneville 2014) for repeat annotation in combination with Repbase v21.05 (Bao et al. 2015). For de novo identification, we predicted repeat regions in primary contigs of Pst_104E_v13 and DK0911_v04 independently using TEdenovo. We combined the resulting de novo repeat libraries with the script “RemoveRedundancyBasedOnCl.py” within the REPET pipeline using the configurations provided in [supplementary data 3](#), [Supplementary Material](#) online. We named the resulting repeat library 104E_p_DK0911_p_classif. We annotated the primary contigs and haplotigs of both assemblies separately using three repeat libraries (repbase2005_aaSeq, repbase2005_ntSeq, and 104E_p_DK0911_p_classif). We generated superfamily classifications as described previously (Schwessinger et al. 2018). (See jupyter notebooks DK0911_TE_filtering_and_summary_p_contigs_fix.ipynb, DK0911_TE_filtering_and_summary_h_contigs_fix.ipynb, Pst_104E_v14_TE_filtering_and_summary_p_contigs_fix.ipynb, and Pst_104E_v13_TE_filtering_and_summary_h_contigs_fix.ipynb in the github repo for full analysis details.)

We analyzed the relative identity distribution of transposable elements (TEs) as proxy of TE age as previously described (Maumus and Quesneville 2014). The average identity and genome coverage per TE family is provided by the REPET pipeline. We used these tables as input and plotted the relative coverage frequency of TE families within average identity

size bins of 1 ([supplementary fig. 1A](#), [Supplementary Material](#) online). We plotted the cumulative difference in TE genome coverage between Pst-104E and Pst-DK0911 against the average TE family identity normalizing the current observed TE coverage difference to one. (See jupyter notebook DK0911_TE_variation_analysis.ipynb for details.)

Gene Model Annotation

We annotated genes on primary contigs and haplotigs independently. We combined RNAseq-guided ab initio prediction using CodingQuarry v2.0 (Testa et al. 2015) and braker v1.9 (Hoff et al. 2016) with de novo transcriptome assembly approaches using Trinity v2.2.0 (Grabherr et al. 2011) and pasa v2.0.1 (Haas et al. 2008). Gene models were unified using evidencemodeler v1.1.1 (Haas et al. 2008) using the weights given in [supplementary data 4](#), [Supplementary Material](#) online.

We mapped the trimmed RNAseq reads described in this study (see above) and previously (Dobon et al. 2016; Schwessinger et al. 2018) against the complete assembly (primary contigs and haplotigs) using hisat2 v2.1.0 (–max-intronlen 10,000 –min-intronlen 20 –dta-cufflinks) (Kim et al. 2015). For ab initio predictions, we reconstructed transcripts using stringtie v1.3.3b (–f 0.2) (Pertea et al. 2015). We ran CodingQuarry (–d) in the pathogen mode using SignalP4 (Petersen et al. 2011) for secretome prediction on the soft-masked genome using RepeatMasker v4.0.5 (–xsmall –s GC 43). Similarly, we used the stringtie reconstructed transcripts as training set for the ab initio prediction pipeline braker 1 v1.9 (Hoff et al. 2016) and used the nonrepeat masked genome as reference.

We used Trinity v2.2.0 to obtain *P. striiformis* f.sp. *tritici* transcripts both in the de novo mode and in the genome-guided mode. All RNAseq samples contained host and pathogen RNA as they were prepared from infected wheat tissue. We first mapped all reads to the genome using hisat2 (see above). We extracted mapped RNAseq reads using picard tools SamToFastq. Only those reads that mapped against *P. striiformis* f.sp. *tritici* contigs were used in the de novo pipeline of Trinity (–seqType fq). For genome-guided assembly, we used bam files generated with hisat2 as starting point for Trinity (–jacard_clip, –genome_guided_max_intron 10,000). We used the pasa pipeline v2.0.2 to align both sets of Trinity transcripts against *P. striiformis* f.sp. *tritici* contigs with blat and gmap.

The different gene models were combined using evidencemodeler v.1.1.1 to get the initial gene sets for primary contigs and haplotigs. These were filtered for homology with proteins encoded in TEs. We used BlastP to search for homology in the Repbase v21.07 peptides database with an e-value cut-off of $1 \times e^{-10}$. In addition, we used transposonPSI (Bao et al. 2015). We used the outer union of both approaches to remove

genes coding for proteins associated with TEs from our list of gene models.

Protein Annotation

We performed protein annotation as described previously including homology to swissprot proteins (uniref90, downloaded September 22, 2016) (Bairoch and Apweiler 2000), to carbohydrate-active enzymes (dbCAN, downloaded September 22, 2016) (Yin et al. 2012), to peptidases (MEROPS v10.0) (Rawlings et al. 2016) (see jupyter notebooks in the protein_annotation folder on github). We complemented this analysis by interproscan v5.21-60 (-iplookup -goterms -pa) (Jones et al. 2014), eggno-mapper v0.99.2 (-m diamond and -d euk) (Huerta-Cepas et al. 2016), SignalP 3 (Bendtsen et al. 2004), and EffectorP v2.0 (Sperschneider et al. 2016, 2018).

In case of Pst-DK0911 proteins labeled as “candidate effectors” or “EffectorP” belong to the same protein group. They are defined as secreted proteins using SignalP3 followed by being labeled as “candidate effectors”/“effectorP” by the machine-learning program EffectorP v2.0.

In case of Pst-104E, protein grouping was described in detail previously (Schwessinger et al. 2018). Briefly, “effectorP” labeled proteins were defined as above except for using EffectorP v1.0. “Candidate effectors” are the outer union of “effectorP” labeled proteins and secreted proteins that are upregulated in haustoria or during the plant infection process when compared with spore stages.

BUSCO Analysis

We used BUSCO3 to identify core conserved genes and to assess genome completeness (Simão et al. 2015). In all cases, we ran BUSCO3 in the protein mode using the basidiomycota reference database downloaded September 1, 2016 (-l basidiomycota_odb9 -m protein).

Interhaplotype Variation Analysis

We performed the interhaplotype variation analysis similar as described previously (Schwessinger et al. 2018). Trimmed Illumina reads derived from DK0911, Pst_104E, and PST78 were mapped against the genomes (DK0911 and Pst_104E) using BWA-MEM v0.7.15-r1142-dirty using the standard parameters (Li 2013). We called single-nucleotide polymorphisms (SNPs) in bulk using freebays (Garrison and Marth 2012) and following hard filtering by vcf-filter with DP >10 and QUAL > 20 (vcflib 2017). Variants for DK0911, Pst_104E, and PST78 resequencing data were parsed out and summarized with real-time genomic vcfstats v3.8.4 (rtg-tool 2017).

We performed large-scale variation analysis as described previously using nucmer and assemblytics (Kurtz et al. 2004; Nattestad and Schatz 2016). (See jupyter notebooks DK_0911_nucmer_assemblytics_mapping.ipynb, DK_0911_

assemblytics_analysis.ipynb, and DK_0911_Pst104E_assemblytics_plot.ipynb for details.)

Within Genome Allele Variation Analysis

We used proteinortho v5.16 in synteny mode with default parameters (-synteny) to identify alleles between the primary assembly and haplotigs (Lechner et al. 2011). We restricted our analysis to high-quality allele pairs that are located on linked primary contigs and haplotigs. We assessed the variation of high-quality allele pairs by calculating the Levenshtein distance on the codon-based CDS alignments. The pairwise protein alignments were generated with muscle v3.8.31 (Edgar 2004), and converted into codon-based CDS alignments using PAL2NAL v14 (Suyama et al. 2006). Analysis details can be found in jupyter notebook DK0911_vs_Pst104E_gene_pair_analysis.ipynb.

Coverage Analysis and Identification of Unphased Regions in Primary Contigs

We identified unphased regions in Pst-DK0911 as reported previously for Pst-104E (Schwessinger et al. 2018). We performed detailed read depth coverage analysis to obtain a genome level insight into the relative quantity of fully phased, homozygous collapsed, and hemizygous regions in the two *P. striiformis* f.sp. *tritici* genomes. We determined the sequencing depth in 1-kb sliding windows with 200-base intervals. Read depth coverage was calculated by mapping short reads derived from each *P. striiformis* f.sp. *tritici* isolate against its own genome using BWA-MEM v0.7.15-r1142-dirty and the standard parameters (Li 2013). We mapped reads against primary contigs only (p) and both primary contigs and haplotigs (ph). We normalized sequencing depth to one at the main “haploid” sequencing depth peak on primary contigs when mapping against primary contigs and haplotigs. In a perfect fully phased assembly, this is the main sequencing depth peak, because of the absence of any homozygous collapsed regions. We plotted the normalized sequencing depth for primary contigs (both p and ph mapping), haplotigs (ph mapping), regions in primary contigs that have corresponding phased haplotigs and regions in primary contigs without assigned haplotigs. In addition, we used publicly available long-read genomes and corresponding Illumina short reads for three additional *P. striiformis* isolates. This includes *P. striiformis* f.sp. *tritici* 93-210 (SAMN08200485), *P. striiformis* f.sp. *hordei* 93TX-2 (SAMN08200486), and *P. striiformis* 11-281 (SBIN00000000) (Xia et al. 2018; Li, Xia, et al. 2019). (See [supplementary data 5, Supplementary Material](#) online, for SRA identifiers.) For details on analysis specifics, see jupyter notebook DK0911_SRM_cov_DK0911_on_DK0911.ipynb, Pst_104E_SRM_cov_Pst_104E_on_Pst_104E.ipynb, DK0911_Pst104E_comperative_coverage_analysis.ipynb, and 20200129_het_cov_revision_v01.ipynb.

Short-Read k-mer Frequency Analysis to Estimate Levels of Homo- and Heterozygosity

We investigated levels of homo- and heterozygosity directly from short-read sequencing data for several additional *P. striiformis* f.sp. *tritici* isolates linked to recent incursions from the Himalayan region plus appropriate controls (Hubbard et al. 2015; Bueno-Sancho et al. 2017; Schwessinger et al. 2018; Xia et al. 2018; Li, Xia, et al. 2019). We performed k-mer analysis on raw Illumina short-read using jellyfish v2.2.6. We first invoked the count command with the k-mer size of 21 (-m 21) and size of 1,000,000,000 (-s 1,000,000,000). We converted the resulting count file into a histogram using the histo command of jellyfish (Marçais and Kingsford 2011). We plotted k-mer frequency spectrums and estimated heterozygosity using GenomeScope2 online, last accessed February 12, 2020 (Ranallo-Benavidez et al. 2020). (See [supplementary data 5, Supplementary Material](#) online and 20200129_genome_size_revision_v01.ipynb for details.)

Cross-isolate Genome-Wide Presence–Absence Analysis

We aimed at determining presence–absence polymorphism at the whole-genome level. We first mapped short reads derived from one *P. striiformis* f.sp. *tritici* isolate (“query”) against the complete genome (ph) of the other isolate (“subject”) using BWA-MEM v0.7.15-r1142-dirty using standard parameters. We then calculated sequencing depths in 1-kb sliding windows as described earlier. We defined regions that fell <10% normalized sequencing depth in the cross-mapping but not self-mapping experiments as absent in the “query” isolate. We used bedtools (Quinlan and Hall 2010; Dale et al. 2011) to identify genes which are completely contained within these regions and defined them as “variable genes.” We estimated the distribution of the expected number of variable genes using a permutation test randomly reshuffling the absent regions 5,000 times. We used this random distribution to calculate a *P* value testing the hypothesis if the observed number of variable genes is different from the observed random distribution at a *P* value cut-off of 0.05. We performed a similar analysis for TEs with the important difference to determine variable TE content at single base pair resolution and with 2,500 permutations. In addition, we performed similar tests on the variable TE content using reciprocal whole-genome alignments as input. We aligned each genome against each other with the mummer package v4. Initially, alignments with nucmer used -l 20 -c 65 -max-match. Alignments were filtered with delta-filter requiring no uniqueness -u 0 but a minimum sequence identifies of 95% -i 95 (see notebook Mummer_DK0911_Pst_104E.ipynb and DK0911v04_Pst104E_presence_absence.ipynb for more detail). We converted mummer delta files into bed files for input in the presence–absence analysis as described earlier. Details on this analysis can be found in jupyter notebooks

DK0911_SRM_cov_Pst_104E_on_DK0911.ipynb, Pst_104E_SRM_cov_Pst_104E_on_Pst_104E.ipynb, Mummer_DK0911_Pst_104E.ipynb, and DK0911v04_Pst104E_presence_absence.ipynb.

Ortholog Analysis

We performed orthology analysis orthofinder/2.2.6 (Emms and Kelly 2019) of all nonredundant protein sets with publicly available *Pucciniomycotina* genomes. Protein sets were downloaded from MycoCosm (Grigoriev et al. 2014) (see [supplementary data 6, Supplementary Material](#) online, for details). *Zymoseptoria tritici* and *Verticillium dahliae* protein sets were also included as outgroup.

We defined singletons between the two isolates as proteins that were in orthogroups that did not contain a member from the other isolate. We performed enrichment analysis interrogating if different gene categories are enriched for singletons over others. For this, we used Fisher’s exact test and Bonferroni correction executed in python (McKinney 2010). Detailed analysis can be found in jupyter notebook DK0911_vs_Pst104E_synteny.ipynb, Pst104E_vs_DK0911_synteny.ipynb, DK0911_vs_Pst104E_reciprocal_gene_pair_analysis.ipynb, and DK0911v04_Pst104E_presence_absence_orthology.ipynb.

Synteny Analysis

We performed detailed synteny analysis to identify the best reciprocal gene-pairs between the two isolates. In addition, we investigated if certain gene categories are more syntenic than others considering parameters like maximum synteny block size and number of allowed gaps within a synteny block.

We identified best reciprocal gene-pairs as follows. For each orthogroup, we identified the reciprocal gene-pairs or groups belonging to each isolate. If there was more than one gene-pair candidate we identified, then the pair(s) for which each downstream and upstream gene was conserved in terms of orthogroup identity as well. In the case of multiple candidate gene-pairs, we assigned gene-pair status to pairs that formed the longest synteny block when allowing for a maximum synteny gap number of eight.

We identified synteny blocks using MCSanX (Wang et al. 2012) inspired by previous analysis (Zhao and Schranz 2019). We ran MCSanX (Wang et al. 2012) and Diamond (Buchfink et al. 2015) within the Synnet.sh script with following parameters. MCSanX was run fixing the -w flag to 0, the -s flag to 3, and varying the -m flag with the following values: 0, 1, 2, 3, 4, 5, 6, 7, 8, 9, 10, 15, 25, and 35. These settings allow for the identification of synteny blocks involving at least three genes with a varying number of allowed gaps within the synteny block. (See [supplementary fig. 2, Supplementary Material](#) online, for an illustration of gaps within synteny blocks.) Diamond was run with the following flags: -max-hsps 1 -k

25 -f 6 -b 5. Resulting *.collinearity files were parsed and further analyzed as described earlier. Detailed description of downstream analysis can be found in in jupyter notebook DK0911_vs_Pst104E_reciprocal_gene_pair_analysis.ipynb and DK0911v04_Pst104E_presence_absence_orthology.ipynb.

Gene-Pair Variation Analysis

We assessed the variation between the gene-pairs of the two isolates using three approaches. We calculated the Levenshtein distance based on the codon-based CDS alignments and on the protein alignments of each gene-pair. We calculated the dN:dS ratios by using these two alignment sets with yn00 paml version 4.9 (Yang and Nielsen 2000). The protein sequences of each gene-pair were aligned using muscle v3.8.31 (Edgar 2004), and codon-based alignments were generated using PAL2NAL v14 (Suyama et al. 2006). The Levenshtein distance was calculated in python using the distance module v0.1.3. Analysis details can be found in jupyter notebook DK0911_vs_Pst104E_reciprocal_gene_pair_analysis.ipynb.

Telomere Analysis

We estimated telomere length and telomere patterns using computel (Nersisyan and Arakelyan 2015) providing a haploid chromosome number of 18 (-nchr) and the genome size (-lgenome) of the primary assemblies. The haploid chromosome number is based on the observation that closely related rust fungi such as *P. graminis* f.sp. *tritici* (Boehm et al. 1992; Li, Upadhyaya, et al. 2019; Sperschneider et al. 2020) and *Melampsora lini* (Boehm 1992) have 18 chromosomes haploid. Hence, it is the most parsimonious assumption that *P. striiformis* f.sp. *tritici* haploid chromosome number is 18.

Genome Architecture Analysis

We analyzed various features between certain gene families and in regards to TEs using bedtools (Quinlan and Hall 2010) and pybedtools (Dale et al. 2011) as described previously (Schwessinger et al. 2018). (See jupyter notebook DK0911_v04_effector_analysis.ipynb.)

Mitochondrial Genome Assembly, Annotation, and Comparison

To assemble the Pst-DK0911 mitochondrial genome, we extracted mitochondrial reads from whole-genome PacBio reads of Pst-DK0911 by mapping them to the closely related *Phakopsora meibomia* (soybean rust pathogen) mt-genome (Stone et al. 2010) using bwa version 0.7.15-r1140 (Li 2013). The reads were de novo assembled with Canu v1.6 (Koren et al. 2017). Canu produced a single circular contig of ~124 kb. The circularity of the contig was confirmed by dot

plot using Gepard v-1.40 (Krumstiek et al. 2007). This produced a typical dot plot with identical repeats at both ends, indicating a circular topology. The repeated sequences at the ends of the contig were removed and the remainder circularized using circlator v-1.4.0 (Hunt et al. 2015). The final circularized contig was of 101,813 bp. The contig was polished/error corrected with two iterations of long reads using PacBio's GenomicConsensus Arrow (2019, <https://github.com/PacificBiosciences/GenomicConsensus>, last accessed November 4, 2019) and five iterations of Illumina short reads using pilon v-1.22 (Walker et al. 2014). The polished mt-genome was annotated with two independent mt-genome annotation tools, GeSeq web browser, <https://chlorobox.mpimp-golm.mpg.de/geseq.html> (Tillich et al. 2017, last accessed June 5, 2019) using the *Phakopsora* mt-genome as a reference and MITO web server using genetic code 4 <http://mitos.bioinf.uni-leipzig.de/index.py> (Bernt et al. 2013, last accessed June 5, 2019). Annotations using these web browsers were checked individually to confirm gene boundaries as well as intron-exon boundaries by aligning the predicted genes with their orthologs in closely related fungal species. Annotated tRNA genes were further evaluated and compared using tRNAscan-SE v2.0.3 (Lowe and Eddy 1997) and ARAGORN v1.2.38 (Laslett and Canback 2004). Introns were annotated using RNAweasel (Lang et al. 2007). We compared our mitochondrial genome with three previously published mitochondrial genomes that have a similar length of about 100 kb including *P. striiformis* f.sp. *tritici* 93-210 (CM009485), *P. striiformis* f.sp. *hordei* 93TX-2 (CM009486), and *P. striiformis* f.sp. *tritici* CY32 (MH891489) (Xia et al. 2018; Li et al. 2020). We performed whole-genome alignments using LASTZ within Geneious Prime version 2020.0.5. We visually inspected gene annotation between Pst-DK0911 and Pst-CY32.

Results

A High-Quality Partially Haplotype-Phased Genome for Pst-DK0911, a Warrior (PstS7) Isolate

We aimed to generate a haplotype-phased genome of the isolate Pst-DK0911 representing the PstS7 lineage (Ali et al. 2017) generally known as "Warrior" (Hovmøller et al. 2016) using PacBio long reads (supplementary data 7, Supplementary Material online and table 1) assembled with FALCON-Unzip (Chin et al. 2016), which is designed to output haplotype phase blocks (haplotigs) for regions where homologous chromosomes vary significantly. The primary genome assembly of Pst-DK0911 is highly contiguous with 94 contigs and a contig N50 of 1.54 Mb, whereas the haplotigs are far more fragmented consisting of 1,176 contigs. The 94 primary contigs totaled 74 Mb in size and the 1,176 haplotigs constituted a size of 52 Mb (table 1). Here, haplotigs represent

Table 1

Summary of Pst-DK0911 Genome Assembly and Annotation

	Primary Assembly		Haplotype Assembly
	Primary Contigs with Haplotigs	Primary Contigs without Haplotigs	Haplotigs
Number of contigs	86	8	1,176
Bases	73,945,211	482,406	52,126,201
TEs coverage	56.02%	80.90%	51.80%
Number of genes	15,003	67	10,870
Average gene length	1,553	1,032	1,419
Average introns per gene	3.31	1.73	3.12
Number of genes per 10 kb	2.02	1.39	2.08
BUSCOs	1,290 (S: 1,184, D: 50, F: 43)	2 (S: 2)	886 (S: 727, D: 77, F: 56)
Number of BUSCOs per 10 kb	0.17	0.04	0.17
Number of candidate effectors ^a	816	3	557
Number of candidate effectors ^a per 10 kb	0.11	0.06	0.11

NOTE.—Summary statistics for the genome assembly according to the three different contig categories as described in the main text. For the BUSCO annotation, we used the following abbreviations. S, single copy; D, duplicated; F, fragmented.

^aCandidate effectors have been predicted based on the machine-learning algorithm EffectorP2 only.

genome regions where the two haploid genome copies are significantly different. The genome was annotated based on new and previously published expression data from several different developmental and infection stages of *P. striiformis* f.sp. *tritici* on wheat (Dobon et al. 2016; Schwessinger et al. 2018). The Pst-DK0911 genome appears to be complete as measured by the identification of benchmarking conserved single-copy orthologs (BUSCOs, basidiomycota odb9) (Simão et al. 2015). We could identify complete BUSCO hits for 97% (1,290/1,335) of the benchmarking set with only 2% (25/1,335) missing. In addition, the assembly has a low level of duplicated BUSCOs (< 5%) indicating that it is completely phased and that primary contigs do not contain extensive duplicated regions or unassigned haplotigs. This makes our Pst-DK0911 genome assembly high quality and comparable to previous long-read genome assemblies for *P. striiformis* f.sp. *tritici* (Schwessinger et al. 2018; Xia et al. 2018) and therefore suitable for in depth comparative genomics with the other available partial haplotype phase assembly of Pst-104E (Schwessinger et al. 2018). In total, we annotated 15,070 genes on primary contigs and 10,870 genes on haplotigs in Pst-DK0911. The overall gene length (1,550 bp on primary contigs and 1,420 bp on haplotigs) and average number of introns per genes (3.3 and 3.1 for primary contigs and haplotigs, respectively) are similar between primary contigs and haplotigs and near identical to our previous long-read assembly of Pst-104E (table 1) (Schwessinger et al. 2018).

Potential molecular functions of all protein-coding genes were assessed by searches against several databases (see Materials and Methods). About 50% of the proteome contained at least one functional domain (supplementary data 7, Supplementary Material online and table 2). We predicted candidate effectors with the machine-learning program EffectorP 2.0 (Sperschneider et al. 2018) applied to the secretome identified with SignalP 3.0 (Bendtsen et al. 2004). We

identified 819 candidate effectors on primary contigs and 557 on haplotigs.

A High-Quality Mitochondrial Genome for Pst-DK0911

Using PacBio long reads, we were able to assemble a high-quality, circular mitochondrial genome for Pst-DK0911 with a length of 101,813 bp (supplementary fig. 3, Supplementary Material online), which displays a high structural and sequence conservation when compared with three previously published *P. striiformis* mitochondrial genomes (Xia et al. 2018; Li et al. 2020) (supplementary fig. 4, Supplementary Material online). The Pst-DK0911 mt-genome contains 14 protein-coding genes that encode components of the electron transport chain, including three copies of the ATP synthase complex (*atp6*, *atp8*, and *atp9*), seven subunits of the nicotinamide adenine dinucleotide ubiquinone oxidoreductase complex (*nad1*, *nad2*, *nad3*, *nad4*, *nad4L*, *nad5*, and *nad6*), one cytochrome b (*cob*), and three subunits of cytochrome c oxidase (*cox1*, *cox2*, and *cox3*). In addition, the mt-genome encodes a ribosomal protein (*rps3*) which is a frequent component of fungal mt-genomes (Losada et al. 2014; Korovesi et al. 2018), and a set of 24 tRNAs. All coding and noncoding genes are transcribed clockwise by the plus strand only. The protein-coding regions are separated by large (800–2,100 bp) regions containing abundant AT-rich repeats.

The difference in genome size between Pst-DK0911 and Pst-104E, representing two different *P. striiformis* f.sp. *tritici* lineages, is explained by the difference in TE content and suggests a recent TE burst.

The overall genome composition and coding capacity (table 1) of Pst-DK0911 are very similar to that of previous long-read assemblies (Schwessinger et al. 2018; Xia et al. 2018). At the same time, the cumulative size of the primary contigs of Pst-DK0911 is 74 Mb, whereas it is 83 Mb for Pst-104E and

85 Mb for Pst-93-210. We investigated if this difference might be linked to differences in TE content. When analyzing repetitive elements, ~56% of the Pst-DK0911 genome was annotated as encoding TEs, shared equally between Class I and Class II elements (supplementary fig. 2, Supplementary Material online). In the case of Class I retrotransposons, LTR Gypsy and Copia elements were by far the most abundant superfamilies. TEs belonging to the TIR order were the most abundant Class II DNA transposons. The overall distribution of TEs into superfamilies and their relative percentage identity compared with the family consensus sequence in Pst-DK0911 was very similar to what have previously been observed in Pst-104E with the most recent TE amplification peak centering ~90% family level sequence identity (Schwessinger et al. 2018) (supplementary figs. 1A and 5, Supplementary Material online). Here, sequence conservation (identity) can be used as a proxy for TE age (Maumus and Quesneville 2014), so more recent TE duplication events display a greater sequence conservation than older TE copies, indicating that the expansion of TEs in Pst-104E and Pst-DK0911 has happened in recent history.

Yet TE genome coverage was distinct between the two genomes contributing to the difference in primary contig size (approximation of genome size) between Pst-DK0911 (table 1) and Pst-104E (Schwessinger et al. 2018). TE content of Pst-DK0911 was 41 Mb when compared with 47 Mb in Pst-104E, which accounts for a 14% increase in TE content and for 54% of the observed genome size difference between the two genomes. Indeed, there appears to be a specific expansion of TEs in Pst-104E that is absent in Pst-DK0911 (supplementary fig. 1B, Supplementary Material online). About 40% of the difference in TE coverage in Pst-104E relative to Pst-DK0911 is explained by an expansion of TEs with an average sequence identity relative to the family consensus sequence ranging from 82% to 95% (supplementary fig. 1B, Supplementary Material online). It is also the relatively young TE families that demonstrate the largest difference in coverage between Pst-104E and Pst-DK0911, these belong mainly to the Class I LTR Gypsy and unclassified Class II elements (supplementary fig. 1C and D, Supplementary Material online).

Comparatively Low Heterozygosity Levels in Pst-DK0911 Suggest Long-Term Asexual Reproduction Contributes Positively to the Accumulation of Genetic Variations

In addition to a substantially smaller genome size, the Pst-DK0911 genome was phased to a much lower level than Pst-104E, reaching levels of 70% phasing compared with over 90% for Pst-104E (Schwessinger et al. 2018). This suggests that Pst-DK0911 is less heterozygous than Pst-104E, because lower levels of heterozygosity prevent the phasing of haplotypes during the assembly process (Chin et al. 2016). Hence, we tested heterozygosity levels in five independent ways. First, we determined the number of heterozygous

SNPs when mapping Illumina short reads of the same isolate against its primary contigs only. Here, Pst-104E had about 7.1 SNPs/kb (~0.71% variation) which is consistent with previous reports of isolates belonging to the Pst50 and PstS1/2 lineage, for example, Pst 93-210 6.4 SNPs/kb, Pst-21 5.0 SNPs/kb, Pst-43 5.3 SNPs/kb, Pst-130 5.4 SNPs/kb, Pst-87/7 6.6 SNPs/kb, Pst-08/21 7.6 SNPs/kb, and Pst-78 6.0 SNPs/kb (Cantu et al. 2011, 2013; Zheng et al. 2013; Hubbard et al. 2015; Cuomo et al. 2016; Bueno-Sancho et al. 2017; Schwessinger et al. 2018; Xia et al. 2018; Radhakrishnan et al. 2019). In contrast, Pst-DK0911 had only 1.6 SNPs/kb (~0.16% variation), which is dramatically less and consistent with our observation of reduced phasing in the Pst-DK0911 genome assembly. Secondly, we made use of the partially phased assemblies to estimate larger scale variations. When comparing Pst-DK0911 with Pst-104E, we consistently observed that the cumulative variation size in different size bins is always larger in Pst-104E (fig. 1). In total, the larger scale structural variants covered 5.10 Mb (~6.39% variation) in Pst-104E and 2.00 Mb (~2.66% variation) in Pst-DK0911. Third, we analyzed the normalized read mapping coverage of primary contigs and haplotigs to estimate the level of heterozygosity and of hemizygosity versus the level of collapsed regions in the two genome assemblies. We normalized the read mapping coverage to one ("haploid coverage") using completely phased regions of each genome as reference when mapping reads against both primary contigs and haplotigs (fig. 2B and D). When mapping against the primary contigs only (fig. 2A), nearly all regions of the Pst-DK0911 genome displayed two times ("diploid") coverage, suggesting a high level of similarity between the two haplotypes, such that reads from one haplotype are able to map to the other haplotype. In contrast, Pst-104E also showed a peak at 1× coverage which suggests the presence of hemizygous regions in its genome. Indeed, when mapping reads against primary contigs and haplotigs, Pst-104E showed a single strong coverage peak for all regions analyzed (fig. 2B–D) including regions in primary contigs that lack an alternate haplotig. This supports the conclusion that Pst-104E contains hemizygous regions in its genome that are significantly different between the two haploid nuclei. In contrast, nearly all genome regions in Pst-DK0911 which lack a corresponding haplotig display 2× "diploid" coverage indicating that these regions are collapsed in this genome assembly and present in both haploid nuclei. We also made use of three additional available long-read primary genome assemblies of *P. striiformis*, Pst-93-210, Psh-93TX-2, and Ps-11-281 (Xia et al. 2018; Li, Xia, et al. 2019) to investigate if high levels of hemizygous regions are common. Indeed, all three genome assemblies display significant levels of hemizygous regions similar to Pst-104E based on normalized read mapping coverage of primary contigs (supplementary fig. 6, Supplementary Material online). Fourth, we estimated heterozygosity rates based on k-mer frequency profile of Illumina short-read sequencing data. This approach revealed relatively

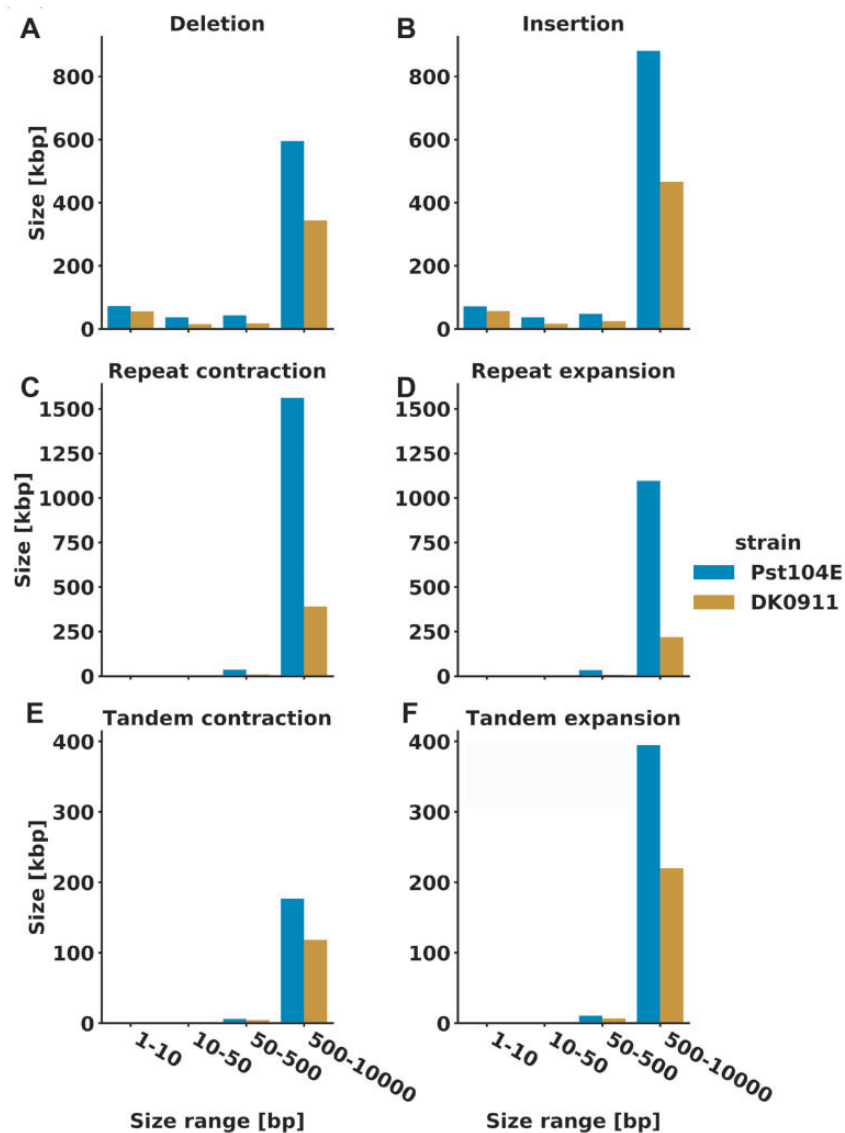


FIG. 1.—Reduced interhaplotype structural variations in Pst-DK0911. Summary of interhaplotype variation between primary contigs and their respective haplotigs, analyzed using Assemblytics. Each plot indicates the number of bases that are spanned by the specific variation category. Pst-DK0911 displays less variation than Pst-104E in all categories.

high heterozygosity rates in Pst-CY32 previously (Zheng et al. 2013) and is exemplified by a double peak in the k-mer frequency profile (fig. 3). This approach enabled us to extend our analysis to four more *P. striiformis* f.sp. *tritici* isolates that have been recently introduced to western wheat growing areas from the Himalayan region (Hubbard et al. 2015; Bueno-Sancho et al. 2017). Overall all five isolates recently derived from the Himalayan region, Pst-DK0911, Pst-11/08, Pst-Kranich, Pst-12/83, and Pst-12/86, display a single k-mer frequency peak when compared with the other non-Himalayan region isolates including Pst-104E (fig. 3 and [supplementary data 5, Supplementary Material](#) online). Fifth, we analyzed the nucleotide variation of high confidence gene-pairs (alleles)

within each assembly (primary contigs vs. linked haplotigs). A total of 52% (7,472/14,321) of all possible high-quality gene-pairs in Pst-104E displayed variation on the CDS level (Levenshtein distance >0) compared with 40% (4,344/10,870) in Pst-DK0911. The distribution of nucleotide variation of high-quality gene-pairs varied significantly between Pst-104E and Pst-DK0911 (median: 0.0053 vs. 0.0012, Mann-Whitney *U* test, *P* value = 3.13e-93) with the first quartiles being more extended in Pst-104E compared with Pst-DK0911, whereas following quantiles are more extended in Pst-DK0911 (fig. 4). This suggests two different potential sources of gene-pair variation. Overall Pst-104E is clearly more heterozygous than Pst-DK0911 in its genome architecture.

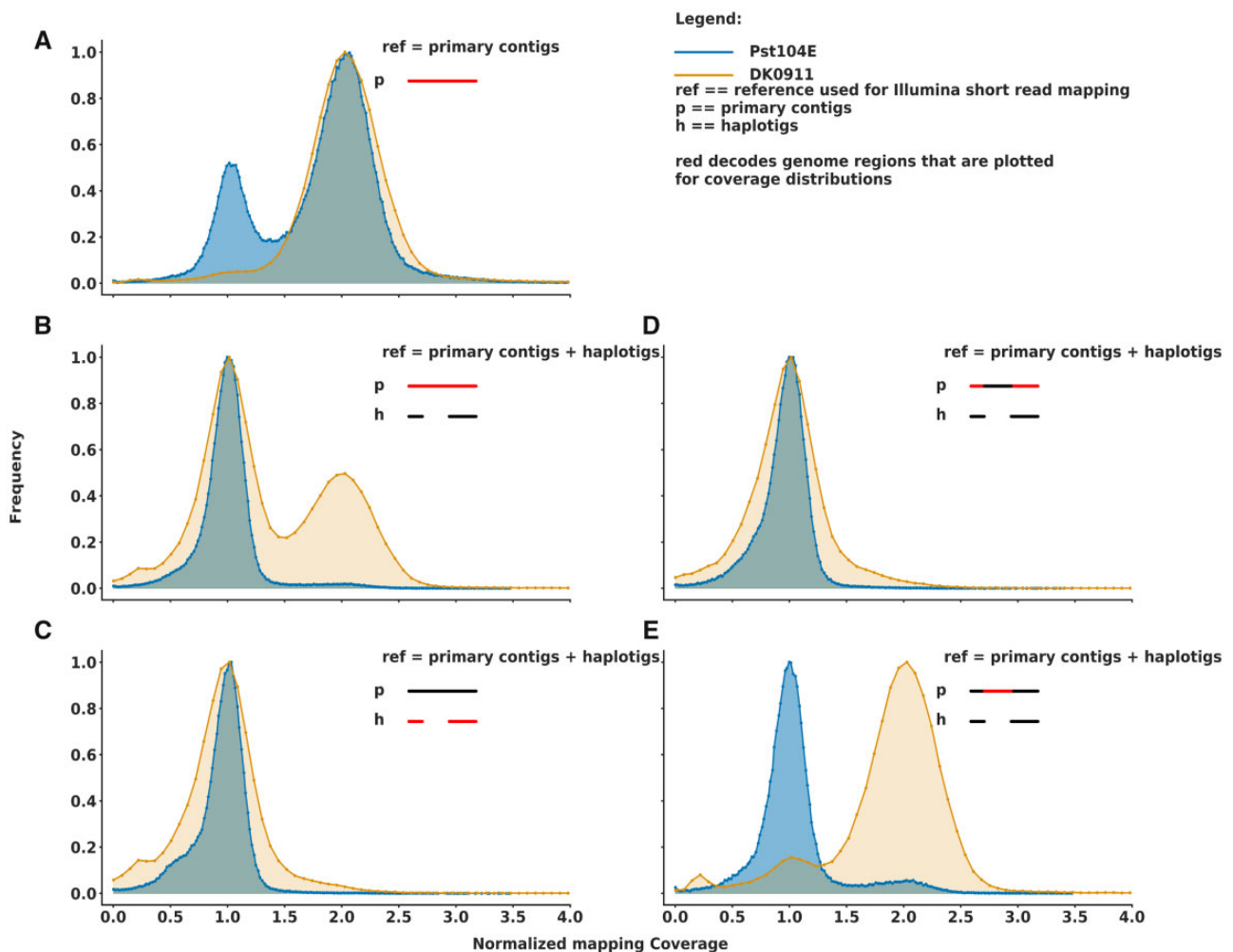


FIG. 2.—Low level of hemizygous regions in Pst-DK0911. Normalized Illumina short-read coverage plots for the red color-coded genome regions in primary contigs when mapping against primary contigs only (A) or when mapping against primary contigs and haplotigs (B, D, and E). (C) Shows the coverage of haplotigs when mapping against primary contigs and haplotigs. Coverage was normalized to one in regions of the genome that are fully phased. The Pst-DK0911 contains significantly less-hemizygous regions when compared with Pst-104E, as it only has a single 2 \times coverage peak when mapping against primary contigs only (A). In addition, nearly all regions in primary contigs that do not possess a corresponding haplotig have 2 \times coverage suggesting that these regions are collapsed homozygous regions in the assembly and not hemizygous (E).

Reduced Telomere Length in Pst-104E Might Be Caused by Long-Term Asexual Reproduction

It is well known that telomere ends shorten with increasing mitotic cell divisions due to the incomplete replication of chromosome ends in mammalian cells (Aubert and Lansdorp 2008) but this phenomenon is less studied in filamentous fungi (Wang et al. 2014). We tested if telomere length is different in Pst-104E compared with Pst-DK0911 assuming a haploid chromosome number of 18 based on the observation that closely related rust fungi such as *P. graminis* f.sp. *tritici* (Boehm et al. 1992; Li, Upadhyaya, et al. 2019; Sperschneider et al. 2020) and *M. lini* (Boehm 1992) have 18 chromosomes in each nucleus. Our hypothesis was that if Pst-104E has been asexual for a longer time period and hence undergone a greater number of successive mitotic cell divisions,

it should have shorter telomeres than Pst-DK0911. We approximated telomere length via searching the canonical “TTAGGG” telomere repeat and variants thereof in whole-genome Illumina short-read data (see Materials and Methods). We estimated 55 telomere repeats in Pst-DK0911 and 18 in Pst-104E, which suggests significant telomere shortening in Pst-104E. Consistently, the canonical “TTAGGG” repeat accounts only for 76% of all patterns in Pst-104E versus 84% in Pst-DK0911 (see [supplementary data 9, Supplementary Material](#) online, for full analysis results). This suggesting that Pst-104E has accumulated more variations at its telomeres over time. Overall, this observation of relatively short telomeres in Pst-104E compared with Pst-DK0911 is consistent with hypothesis of increased mitotic cell division as suggested by the increased heterozygosity in Pst-104E.

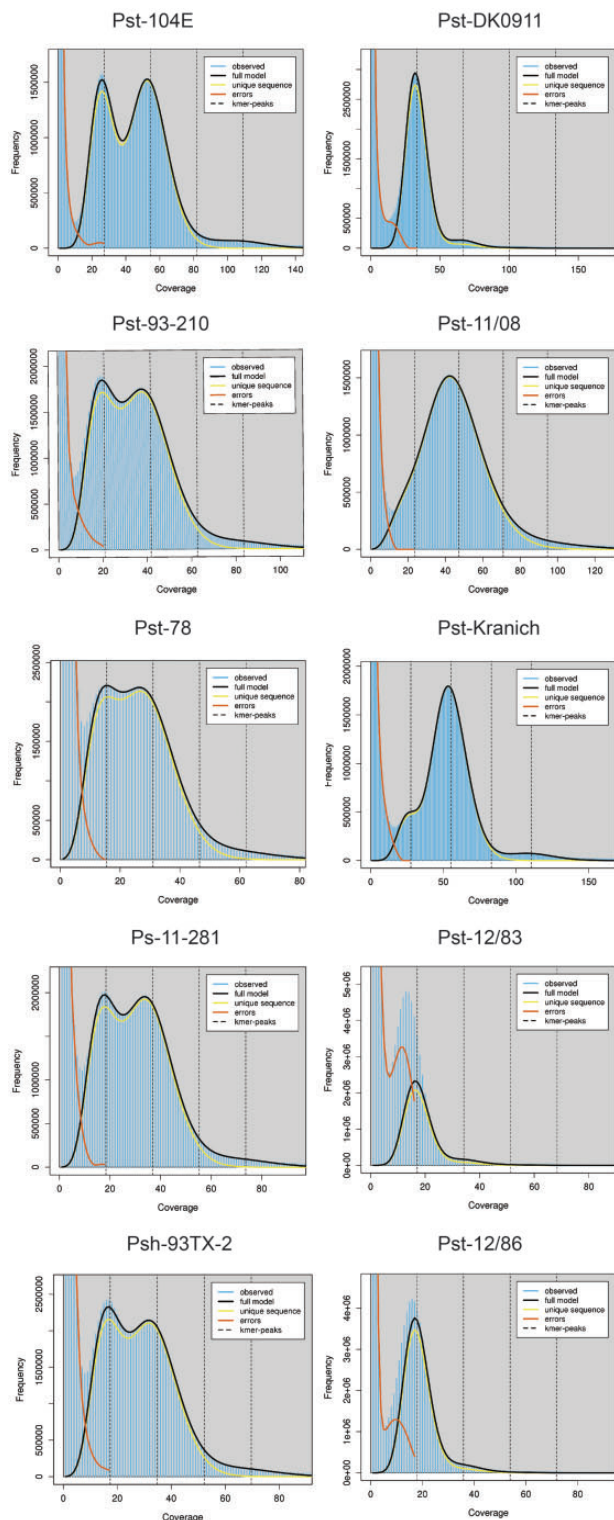


FIG. 3.—Low levels of heterozygosity in four additional *Puccinia striiformis* f.sp. *tritici* isolates linked to the Himalayan region. K-mer frequency plots from Illumina short-read raw data generated with jellyfish and GenomeScope2. High levels of heterozygosity are exemplified by double peaks in the k-mer frequency profile as shown for isolates in the left column including Pst-104E, Pst-93-210, and Pst-78. High levels of

Interlineage Genome Variation Is Dominated by Variation in TEs

Next, we tested for variation and presence–absence polymorphisms between the Pst-104E and Pst-DK0911 genomes using a conservative coverage-based read mapping approach. We defined unique regions (highly variable or absent) in one genome if they fell below a 10% normalized coverage threshold in cross-mapping (e.g., Pst-104E reads onto the Pst-DK0911 genome), but not self-mapping (e.g., Pst-104E reads on to the Pst-104E genome) experiments. In total, we identified 6 Mb of sequence that was unique to Pst-DK0911 and 21 Mb to Pst-104E. We then considered how many genes are completely contained in these unique regions. We identified 724 variable genes that were in the Pst-DK0911 genome and not covered by Pst-104E reads and hence absent in Pst-104E. Conversely, we identified 2,394 variable genes of Pst-104E that were not covered by Pst-DK0911 reads and hence missing from Pst-DK0911. When analyzing if any specific gene group is enriched or depleted within this variable gene set, we found that BUSCOs are significantly depleted in both cases (multiple testing corrected Fisher's exact test P value = 3.1×10^{-11} for Pst-DK0911 and P value = 8.2×10^{-9} for Pst-104E as reference), which is expected for genes that belong to the highly conserved core genome. We could not find any significant enrichment signal for candidate effectors or secreted proteins in either Pst-104E or Pst-DK0911. On the contrary, genes encoding for secreted proteins appeared to be depleted from the Pst-104E variable gene set (multiple testing corrected Fisher's exact test P value = 2.2×10^{-5}).

We next tested if the unique regions were randomly distributed across the genomes or if they contained a different number of genes than expected by chance. To do this, we performed a permutation test by randomly reshuffling the unique regions to establish the expected distribution of variable genes when the unique regions are randomly distributed. In both cases, BUSCO genes were significantly depleted from unique regions (supplementary fig. 7, Supplementary Material online). In the case of Pst-DK0911, candidate effectors and genes encoding secreted proteins were also depleted from unique regions. In contrast, more genes than expected by chance were fully contained within the unique genome regions of Pst-DK0911 and hence absent from Pst-104E. The reverse analyses did not reveal any strong signal for any

FIG. 3.—Continued

homozygosity are exemplified by a single peak in the k-mer frequency profile as shown for isolates in the right column including Pst-DK0911, Pst-11/08, and Pst-Kranich. All isolates in the right column are directly linked to the recent incursion event derived from the Himalayan region. The x axis displays k-mer coverage and is dependent on the sequencing depth of the Illumina sequencing library. (See supplementary data 5, Supplementary Material online, for SRA identifiers and links to full GenomeScope2 reports.)

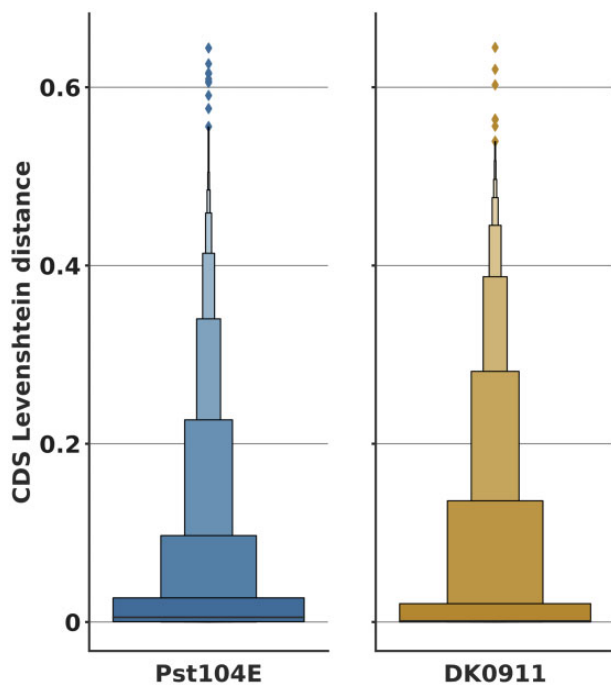


FIG. 4.—Different levels of allelic gene-pair variation in Pst-DK0911. Boxenplot of Levenshtein edit distance of coding regions of high-quality allelic gene-pairs in Pst-104E and Pst-DK0911. For values >0 , $n[\text{Pst-104E}] = 7,472$ and $n[\text{Pst-DK0911}] = 4,344$.

gene group except for genes encoding for BUSCOs and secreted proteins which were significantly depleted from unique regions in Pst-104E. Next, we tested if TEs contribute to sequence variation between the two genomes using a similar approach (see Materials and Methods for details). Indeed, TEs were significantly enriched in unique regions identified by our coverage-based read mapping approach (supplementary fig. 8A and B, Supplementary Material online). As read mapping is known to suffer in repetitive regions, we performed identical tests based on whole-genome alignments allowing for multi-mapping with a percentage identity coverage cut-off of 95%. Consistently, this second independent method also identified that TEs are highly enriched in unique regions in both genomes (supplementary fig. 9A and B, Supplementary Material online). Overall, these analyses suggest that sequence variation between the two isolates is mostly caused by variation in TE sequences.

Interlineage Gene Content Variation Does Not Favor Candidate Effectors

Similar to previous observations in *P. striiformis* f.sp. *tritici* (Schwessinger et al. 2018; Xia et al. 2018) and other rust fungi (Duplessis et al. 2011; Miller et al. 2018), candidate effectors did not show any obvious genome compartmentalization in Pst-DK0911 (supplementary fig. 10, Supplementary Material online). Candidate effectors were not located in gene sparse

regions or linked to TEs. Yet similar to Pst-104E, candidate effectors appeared to be slightly closer to BUSCOs than to other genes (supplementary fig. 10, Supplementary Material online). Next, we tested if candidate effectors are more variable between the two isolates compared with all genes. We performed gene family (orthology) analysis with OrthoFinder (Emms and Kelly 2019) using 59 fungal proteomes representing 38 fungal species with a focus on rust fungi (see supplementary data 6, Supplementary Material online, for details). Overall, candidate effectors did not appear to be significantly enriched in the singleton gene pool of either isolate. When identifying genes without orthologs in one of the two isolates, a total of 1,275 and 1,404 proteins were singletons in Pst-DK0911 and in Pst-104E, respectively. As expected BUSCOs are depleted from the singleton sets in both genomes (multiple testing error corrected Fisher's exact test P value = 3.0×10^{-33} for Pst-DK0911 and P value = 5.3×10^{-31} for Pst-104E). When we investigated the EffectorP predicted candidate effector subset in Pst-104E, we saw a weak signal of enrichment in the singleton gene set (multiple testing error corrected Fisher's exact test P value = 1.0×10^{-4}). In contrast, genes belonging to the secretome were depleted from the singleton gene set in Pst-DK0911 (multiple testing error corrected Fisher's exact test P value = 4.6×10^{-7}).

Candidate Effectors Fall into Conserved and Hypervariable Categories

Although candidate effectors were not specifically enriched in presence-absence polymorphisms between Pst-DK0911 and Pst-104E, we tested whether some of the candidate effectors displayed signs of positive selection. First, we investigated the variation between syntenic orthologs on the nucleotide and amino acid level. About 44% and 57% of all effector candidates displayed variation at the nucleotide level, which is slightly below the genome average of 65% in Pst-DK0911 and 70% in Pst-104E, respectively. The variation between candidate effector genes was higher than BUSCOs but similar to the overall gene pool (fig. 5A, see supplementary data 10–13, Supplementary Material online, for statistical testing and gene category annotation). This trend was very similar at the protein level with 36% and 52% of candidate effectors displaying variation in Pst-DK0911 and Pst-104E, respectively. The variation in BUSCOs was significantly reduced compared with all other gene groups, yet similar between all other gene groups. This suggests that candidate effectors are not distinct from other gene-pairs showing overall similar levels in sequence conservation between isolates. Lastly, we calculated the dN:dS ratio for all syntenic ortholog gene-pairs. Indeed, 51 and 133 candidate effectors displayed a dN:dS ratio greater than one and hence a strong signal for positive selection in Pst-DK0911 and Pst-104E, respectively.

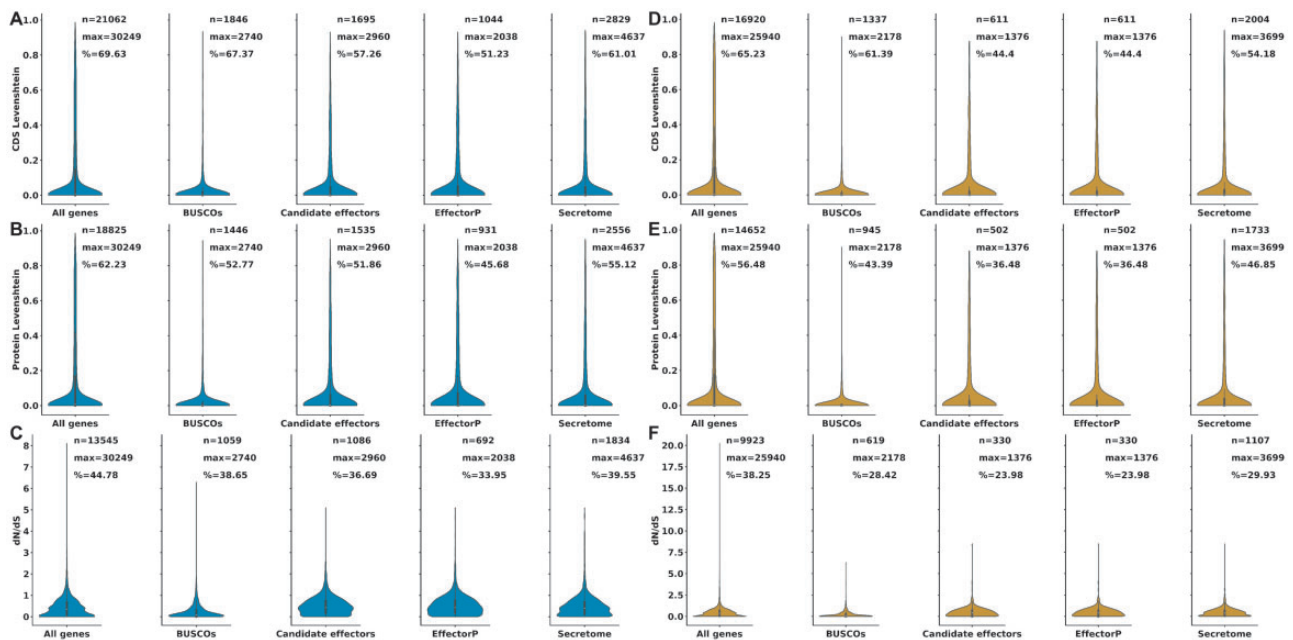


FIG. 5.—A subset of effector candidates displays patterns of positive selection. Violinplots of the pairwise comparison of syntentic orthologs in Pst-104E and Pst-DK0911 split according to gene classifications. (A) Shows the Levenshtein distance at the coding sequence level (CDS). (B) Shows the Levenshtein distance at the protein level. (C) Shows the dN:dS ratio. *n*, number of orthologs genes or proteins with any difference; max, the total number of orthologous genes or proteins; %, the percentage of orthologs genes or proteins with any variation >0. (See the Materials and Methods section for the definition of different gene categories; see [supplementary data 10 and 11, Supplementary Material](#) online, for detailed statistical analysis of the complete data set.)

Candidate Effectors Do Not Show Strong Signals for Altered Synteny

Although candidate effectors are not compartmentalized in rust fungi, we aimed to explore other signals of specific genome organization in regard to candidate effectors in *P. striiformis* f.sp. *tritici*. The availability of two highly contiguous partially phased genomes enabled us to ask the question if candidate effectors displayed an altered synteny pattern similar to *R* genes in plants. *R* genes in plants are the least syntentic genes in land plants (Zhao and Schranz 2019). If this were the case for effectors, it could indicate that candidate effectors are in genomic regions with higher recombination rates or general higher plasticity leading to disruption of gene synteny. Using a similar approach as described for syntentic gene orthologs in plants (Zhao and Schranz 2019), we first tested how sensitive different gene groups are toward allowing a varying number of gene gaps within synteny blocks using primary contigs as queries against the complete assembly as subject. As expected (Zhao and Schranz 2019), BUSCOs were the least affected by the number of gaps (fig. 6). The number of BUSCOs within a synteny block plateaued at about 97% already at a maximum gap size of 2 or 3 in Pst-DK0911 or Pst-104E, respectively (fig. 6A). In contrast, for all other gene groups, the percentage of genes contained in synteny blocks kept on increasing until the maximum tested allowed gap size of 35. Over 94% and 91% of all candidate effectors were contained within synteny blocks with a gap size of 8 or more in Pst-DK0911 or Pst-104E,

respectively. This is more than the genome average of 88% and 86%, respectively. Hence overall candidate effectors do not appear to be less syntentic than the genome average. This observation was further supported by the fact that we observed very little difference in the mean best synteny block length at various numbers of allowed gaps within the alignments (fig. 6B). Although BUSCOs appeared to have slightly longer mean synteny block length, the variation of synteny block length was significant in each gene group (see [supplementary fig. 11, Supplementary Material](#) online) not allowing for any generalization. Overall, these observations are consistent with the fact that candidate effectors are also not enriched in interlineage singletons and appear to be mostly surprisingly conserved at the gene level.

Discussion

Genomic Insights into the Genetic Effects of Sexual Reproduction in *P. striiformis* f.sp. *tritici*

In the early 2010s, *P. striiformis* f.sp. *tritici* isolates from the “Warrior” (PstS7) lineage arrived in Europe severely impacting wheat production by causing stripe rust on previously resistant wheat varieties (Hubbard et al. 2015; Hovmøller et al. 2016). The Pst-DK0911 isolate analyzed in this article belongs to the PstS7 lineage and was captured in Denmark in June 2011 (Hovmøller et al. 2016). The PstS7 lineage is genetically distinct from the pre-existent globally important lineages such as

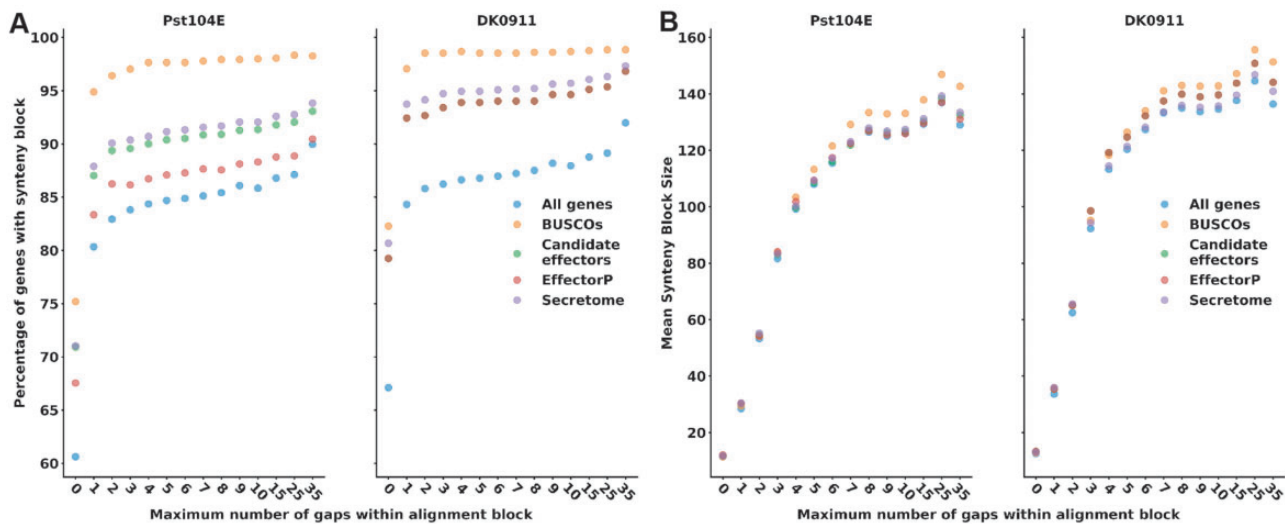


FIG. 6.—Candidate effectors are mostly syntenic between the two *Puccinia striiformis* f.sp. *tritici* isolates. (A) Shows the percentage of genes that are syntenic at increasing number of allowed gaps within the synteny block. (B) Shows the mean synteny block length at increasing number of allowed gaps within the synteny block. The minimum synteny block size is 3. Data points only include genes on the primary contig of the query genome. Data points represent different gene classifications. (See the Materials and Methods section for the definition of different gene categories; see [supplementary fig. 2, Supplementary Material](#) online, explaining the influence of gap size on synteny blocks.)

PstS0 and PstS1/2, which are part of presumed asexual lineages at least tracing back to isolates in Europe in the 1950s (Thach et al. 2016) and Africa in the 1980s (Walter et al. 2016), respectively. Pst-DK0911 in contrast is closely related to sexual *P. striiformis* f.sp. *tritici* populations in the Himalayan regions, which represent the center of genetic diversity for *P. striiformis* f.sp. *tritici* (2017). Pst-DK0911 is one of very few reported *P. striiformis* f.sp. *tritici* isolates that has undergone the complete sexual cycle under laboratory conditions (Rodriguez-Algaba et al. 2014). Self-crosses of Pst-DK0911 suggest that this isolate is largely homozygous, in terms of having two recognized alleles, for several recognized effector loci as none of the tested progeny isolates was able to infect wheat differential lines that were resistant to the parental isolate. Hence, we hypothesize that Pst-DK0911 originated from a highly inbred population that potentially might have undergone several rounds of selfing or crosses between highly related genotypes leading to relatively low heterozygosity. Indeed, our data support this hypothesis as Pst-DK0911 displays the lowest heterozygosity at the SNP level of any *P. striiformis* f.sp. *tritici* isolate analyzed so far and four additional isolates recently arrived from the Himalayan region show similar low heterozygosity levels based on k-mer frequency plots. In addition, Pst-DK0911 displays about half the interhaplotype structural variation when compared with Pst-104E, which belongs to the long-term asexual lineage PstS0. This observation is consistent with the insight gained from *Puccinia coronata* f.sp. *avenae* where the genome of an isolate closely related to sexual populations displays reduced heterozygosity by comparison to the genome of an isolate more closely related to long-term asexual populations (Miller et al. 2018). It is

likely that repeated sexual cycles of *P. striiformis* f.sp. *tritici* lead to reduced heterozygosity as the physiology of sexual reproduction favors inbreeding within one population. In addition, sexual recombination allows for gene conversion and unequal crossover at homologous sides including TEs (Liu et al. 2018; Underwood and Choi 2019). Interestingly, the variation analysis of high-quality gene-pairs in Pst-DK0911 revealed that its genome harbors discontinuous populations of gene-pairs. In general, variation in gene-pairs in dikaryotic rust fungi can be caused by two major factors. The first would be continuous accumulation of mutations during asexual reproduction cycles leading to linear accumulation of variation between gene-pairs. The second being variation that has been introduced at a given point in time, for example, mating of two genetically distinct parents or somatic recombination via the transfer of single nucleus. The gene-pair variation in Pst-DK0911 appears to be shaped by both sources of variation and is best explained by an initial cross of genetically distinct parents, several rounds of selfing of closely related individuals on barberry, followed by a limited number of asexual reproduction cycles on wheat.

The High-Quality Mitochondrial Genome of *P. striiformis* f.sp. *tritici* DK0911 Reveals Long Low Complexity at Regions

The mitochondrial genome of Pst-DK0911 consists of extensive intergenic regions interspersed with long low-complexity AT repeats. The overall structure and gene content of the Pst-DK0911 are consistent with a recently high-quality mitochondrial genome of Pst-CYR32 (Li et al. 2020). Comparative

analysis of *P. striiformis* f.sp. *tritici* mt-genome with rust and other fungi revealed that these repeats are unique to *P. striiformis* f.sp. *tritici* mt-genome. The overall GC content of the *P. striiformis* f.sp. *tritici* mt-genome is 31% rising to 35.8% in the protein-coding regions. This is similar to other fungal mt-genomes (Stone et al. 2010; Torriani et al. 2014), although the *P. striiformis* f.sp. *tritici* mt-genome is comparatively large. The size of fungal mt-genomes can vary by as much as 10-fold; for example, the smallest reported fungal mt-genome is just 20,063 bp for *Candida glabrata* (Koszul et al. 2003) and the largest 230,000 bp for *Rhizoctonia solani* (Losada et al. 2014). The genetic content of these mt-genomes is largely conserved and consists of 14 genes with the order of the genes being highly variable between different fungi. This variability in gene order is the highest in basidiomycete fungi (Aguileta et al. 2014). The gene order of *P. striiformis* f.sp. *tritici* mt-genome is similar to the close relative basidiomycete *Phakopsora* sp., but the order of tRNA genes varies (Stone et al. 2010). Overall, this high-quality reference genome will enable the analysis of mitochondrial inheritance in *P. striiformis* f.sp. *tritici* in future studies.

The Potential Effects of Long-Term Asexual Reproduction on Genome Expansion, Heterozygosity, and Fitness in *P. striiformis* f.sp. *tritici*

In contrast to Pst-DK0911 (Rodriguez-Algaba et al. 2014), isolates belonging to the long-term asexual lineages of PstS0 and PstS1/2 are often compromised in teliospore production on wheat when compared with isolates from regions with signs of sexual reproduction such as China, Nepal, and Pakistan (Ali et al. 2010). Teliospore production is the entry point into the sexual infection cycle on barberry. It was hypothesized that this reduction is caused by counterselection of genes contributing to sexual reproduction in these two lineages given their likely exclusive asexual reproduction over multiple decades (Rodriguez-Algaba et al. 2014). Interestingly, our read cross-mapping presence–absence analysis identified a nonrandom distribution of genes located in highly variable regions of Pst-DK0911 compared with Pst-104E. These and other highly variable genes might be involved in sexual reproduction in Pst-DK0911. In the future, it will be interesting to investigate expression patterns of these genes during teliospore production on wheat and during the sexual cycle of *P. striiformis* f.sp. *tritici* on barberry.

Overall, our comparative analysis suggests that long-term asexual reproduction in Pst-104E has led to a continuous accumulation of mutations, structural variations and a high level of heterozygosity between the two dikaryotic nuclei. The observed gene-pair variation pattern in Pst-104E is distinct compared with Pst-DK0911 and best explained by the continuous accumulation of mutations during asexual reproduction without other major events introducing genetic diversity. Of course, we cannot exclude a somatic hybridization event in

Pst-104E's distant past similar to what has been recently suggested for *P. striiformis* (Lei et al. 2016) and clearly demonstrated at the whole-genome level for the *P. graminis* f.sp. *tritici* isolate Ug99 (Li, Upadhyaya, et al. 2019). In either case, the extensive relative telomere shortening in Pst-104E does support the hypothesis of an extensive number of mitotic cell divisions without interruption by meiosis as telomere shortening is an indication of aging in other organisms (Aubert and Lansdorp 2008). Long-term asexual reproduction and independent accumulation of mutations in both nuclei might have also impacted Pst-104E's overall fitness. This effect of accumulation of mutations in asexual "diploids" is often referred as the Meselson effect (Weir et al. 2016) and might at least in part explain the rapid replacement of the PstS0 lineage by novel incursion, for example, in Australia in the early 2000s (Wellings 2007).

Another striking fact is the relative genome size increase in Pst-104E which is partially (~54%) explained by the expansion of the absolute TE content in this isolate. The contribution of TE expansion to genome size increase is well documented for plants, animals, and fungi. The overall TE family identity profile (TE "age") is not different between Pst-104E and Pst-DK0911 with a most recent peak centering ~80% sequence identity at the family level. This indicates that TEs expansion in Pst-104E and Pst-DK0911 has happened in recent history. This is distinct to other fungal pathogen belonging to the class of *Leotiomycete* where major TE bursts can be observed at various TE "ages." For example, there has been a very recent TE burst in *Blumeria graminis* f.sp. *hordei* DH14 with TE family level sequence identity of >95%. At other end of the spectrum, *Rhynchosporium commune* and *Rhynchosporium secalis* only display a relative old TE burst with average sequence identity at the TE family level of ~65% (Frantzeskakis et al. 2018).

In our case, most of the TE content difference between the two isolate coincides with the major TE burst at ~80% TE family identity. The difference in TE content could be either explained by selective purging of TEs via unequal crossovers during meiosis (Shirleen Roeder 1983) in Pst-DK0911 in its recent past during sexual reproduction cycles. This hypothesis is most parsimonious with the observed data. Alternatively, the extended asexual reproduction cycles in Pst-104E might have led to an increase in TE content in the absence of TE purging and continuous TE activity during infection. The latter has been recently shown for *Z. tritici* in which specific TE families are expressed during the infection of wheat (Fouché et al. 2020). The upregulation of specific TE families during infection was isolate specific, which could explain the difference of relative abundance of some TE families over others. Indeed, TEs are the most variable genomic regions between Pst-DK0911 and Pst-104E as measured at the superfamily level. In the future, it will be important to explore the expression of TEs in several *P. striiformis* f.sp. *tritici* isolates during the infection of wheat. In addition, it would be fascinating to perform

whole-genome comparative analysis of a time series of Pst50 isolates available in the Stubbs collection ranging from the 1950s to the 1990s (collected by R.W. Stubbs, Wageningen University) and later on expanded until today by the Global Rust Reference Center (Thach et al. 2015). These analyses could directly reveal the impact of long-term asexual reproduction on genome architecture, heterozygosity, and TE movement and plasticity.

Effector Evolution in *P. striiformis* f.sp. *tritici* and Beyond

Clearly candidate effectors are not compartmentalized or linked to TEs in *P. striiformis* f.sp. *tritici* (Schwessinger et al. 2018; Xia et al. 2018). The availability of two haplotype-aware assemblies allowed us to test if candidate effectors behave differently compared with other genes in terms of synteny. Overall, candidate effectors did not behave strikingly differently from all genes. Yet comparison between candidate effectors and secreted proteins revealed that fewer candidate effectors, and especially EffectorP predicted candidates, are within a synteny block at any given allowed gap size. This might suggest that these genes have a higher turn-over in regions of the genome that have increased recombination rates. Future studies capturing more of the genetic diversity of *P. striiformis* f.sp. *tritici* with haplotype-aware assemblies will answer if this trend of reduced synteny of candidate effectors holds true in general. Overall, candidate effectors were well conserved between our two isolates and not enriched in presence-absence polymorphisms. Yet we could observe two distinct populations of candidate effectors. About 70% of all candidate effectors were invariable between the two isolates. These might be core effectors required for plant infection of this obligate biotroph with a focus on wheat or not under selection by the plant immune system within the experienced environments. At the same time the remaining set of candidate effectors displayed an increased level of variation and dN:dS ratios, which is likely caused by specific selection pressures exerted by the plant immune system. This was especially visible in Pst-104E. This is consistent with the fact that Pst-104E is more heterozygous with more distinct candidate effector genes reducing the reciprocal mapping rate compared with Pst-DK0911. Overall the difference effector repertoire between Pst-104E and Pst-DK0911 might explain the differences in virulence profiles or aggressiveness observed between these two *P. striiformis* f.sp. *tritici* lineages (Ali et al. 2017).

Evolution of Wheat Rust Fungi

Genome compartmentalization of effectors is absent in rusts (Duplessis et al. 2011; Miller et al. 2018; Schwessinger et al. 2018; Xia et al. 2018), in most other obligate biotrophic plant pathogens including mildews of wheat and barley (Frantzeskakis et al. 2018; Frantzeskakis, Németh, et al. 2019; Fletcher et al. 2019; Müller et al. 2019) and several

other oomycete and fungal pathogens such as *Ramularia collo-cygni* (Frantzeskakis, Németh, et al. 2019; Frantzeskakis, Kusch, et al. 2019; Stam et al. 2018). This suggests that the two-speed genome compartmentalization is not universal and less common than initially anticipated (Frantzeskakis, Kusch, et al. 2019). This poses the question of what other genetic mechanisms lead to variation in candidate effector complements within and between *P. striiformis* f.sp. *tritici* lineages. It has been shown recently that candidate effectors are enriched in recombination hotspots in *Z. tritici* (Grandaubert et al. 2019) and *Blumeria graminis* f.sp. *tritici* (Müller et al. 2019). Similarly, recombination within sexual populations in the Himalayan region could lead to reshuffling of candidate effector loci in *P. striiformis* f.sp. *tritici*. This might bring together the most suitable candidate effectors for infection of wheat lines currently grown on large acreages. Indeed, we hypothesize that *P. striiformis* f.sp. *tritici* undergoes a two-step selection process. First, candidate effector allele combinations must be suited to the infection of modern wheat varieties in contrast to strains only adapted to local barberry populations and the proximal grasses, which are likely regular hosts of *P. striiformis* f.sp. *tritici* within the region. Second, once a *P. striiformis* f.sp. *tritici* lineage is adapted to modern wheat varieties, it must overcome the specific resistance genes within currently grown wheat varieties (Ali et al. 2017). This second step of adaptation is driven by genetic variation introduced during the asexual reproduction cycle of wheat. The mutations in recognized effectors can be caused by SNPs, small insertions and deletions, larger structural variations, and TE movement. Because it is presumed that both nuclei evolve independently during asexual reproduction, recognized effectors that are heterozygous to begin with are highly likely to be lost during this process. This effect is illustrated by the two cloned recognized effectors of *P. graminis* f.sp. *tritici*, AvrSr35 and AvrSr50, which were both heterozygous in the isolates they were identified in Chen et al. (2017) and Salcedo et al. (2017).

A third genetic mechanism of introducing variation is hybridization between distinct species or lineages (Stukenbrock 2016). Hybridization leads to novel allele combinations and previously heterozygous recessive alleles to be unearthed. Interspecies hybridization is important for the emergence of new plant pathogens as demonstrated for *Blumeria graminis* f.sp. *triticeae*, which arose from a cross between *B. graminis* f.sp. *tritici* and *Blumeria graminis* f.sp. *secali* (Menardo et al. 2016). A special form of hybridization is the swapping of whole nuclei between different dikaryotic rust isolates (Park and Wellings 2012). This process is referred to as somatic hybridization and has long been speculated upon based on low-resolution genetic and biochemical markers or novel virulence profiles emerging during coinfection of asexual hosts (Park and Wellings 2012; Lei et al. 2016). Yet only very recently, somatic hybridization has been conclusively demonstrated to be important for wheat rust evolution under

natural conditions. A recent study used completely haplotype-phased assemblies to show that the hypervirulent *P. graminis* f.sp. *tritici* Ug99 isolate is a product of nuclei swapping between isolates of an old South African and a poorly described Iranian *P. graminis* f.sp. *tritici* lineage (Li, Upadhyaya, et al. 2019). It is likely that similar somatic hybridization events occur in *P. striiformis* f.sp. *tritici*. Somatic hybridization of *P. striiformis* f.sp. *tritici* circumvents the first adaptation process on wheat as each haploid nucleus is likely already adapted to wheat. In addition, it can rapidly generate novel effector allele combinations and drive rapid *R* gene adaptation by introducing heterozygosity to the effector gene profile. In addition, the impact of somatic hybridization on generating hypervirulent wheat rust strains increases with the number of genetically distinct lineages within a given location. This furthers the biosecurity risk of higher rates of novel pathotype incursions in wheat growing areas globally.

Conclusions

The future of wheat rust and *P. striiformis* genomics lies in generating complete haplotype-phased genomes that assort each set of chromosomes into specific karyotypes. This will enable us to predict the potential of generating novel allele combinations during the asexual reproduction cycle via mutations and somatic hybridization. In addition, haplotype-phased genomes will facilitate the cloning of recognized effectors. In combination, this will enable us to better detect specific recognized effector allele pair combinations using modern long-read DNA sequence approaches and enable us to better model the durability of certain *R* gene stacking approaches. Lastly, it will be important to survey *P. striiformis* populations in the Himalayan regions, which are not adapted to modern wheat varieties but to locally growing wheat and grasses. This will provide insight into the true genetic diversity of *P. striiformis* and enable us to catalog the entire genetic diversity of effectors. In addition, we might identify effectors that are important for the infection of wheat or those that are negatively selected for by modern wheat varieties.

Supplementary Material

Supplementary data are available at *Genome Biology and Evolution* online.

Acknowledgments

We thank Ben Auxier, Dr Jeff Ellis, Dr Remco Stam, and two anonymous reviewers for excellent comments and suggestions. We also thank Dr Diane Saunders for immediately sharing Illumina raw read data for Pst-12/83 and Pst-12/83. The research on Pst-DK0911 conducted at Aarhus University was funded by the Danish Innovation Fund (Grant No. 11-116241,

RUSTFIGHT). This work was supported by an Australian Research Council DECRA (DE150101897) and Future Fellowship (FT180100024) to B.S.

Author Contributions

The experimental work on Pst-DK0911 was made by Y.-J.C. and C.K.S. under the supervision of A.F.J. and M.S.H. Preliminary bioinformatic analyses of short-read Illumina genomic and transcriptomic data for Pst-DK0911 were made by Y.-J.C. and J.K.V. Provision of a genetically pure stock of Pst-DK0911 and virulence phenotyping of Pst-DK0911 were made by M.S.H. B.S. conducted all bioinformatic analyses except for the mitochondrial genome assembly. R.T. contributed to bioinformatic analysis. R.N. analyzed the mitochondrial genome. All authors contributed intellectually to this study. B.S. wrote the article with contributions from Y.-J.C., A.F.J., R.N., and J.P.R. All authors commented on drafts of this article and approved the final submission.

Literature Cited

- Aguileta G, et al. 2014. High variability of mitochondrial gene order among fungi. *Genome Biol Evol.* 6(2):451–465.
- Ali S, et al. 2016. CloNcaSe: estimation of sex frequency and effective population size by clonemate re-sampling in partially clonal organisms. *Mol Ecol Resour.* 16(4):845–861.
- Ali S, et al. 2017. Yellow rust epidemics worldwide were caused by pathogen races from divergent genetic lineages. *Front Plant Sci.* 8.
- Ali S, Gladieux P, Leconte M, et al. 2014. Origin, migration routes and worldwide population genetic structure of the wheat yellow rust pathogen *Puccinia striiformis* f.sp. *tritici*. *PLoS Pathog.* 10(1):e1003903.
- Ali S, Leconte M, Walker A-S, Enjalbert J, de Vallavieille-Pope C. 2010. Reduction in the sex ability of worldwide clonal populations of *Puccinia striiformis* f.sp. *tritici*. *Fungal Genet Biol.* 47(10):828–838.
- Altschul SF, Gish W, Miller W, Myers EW, Lipman DJ. 1990. Basic local alignment search tool. *J Mol Biol.* 215(3):403–410.
- Anikster Y. 1986. Teliospore germination in some rust fungi. *Phytopathology* 76(10):1026.
- Aubert G, Lansdorp PM. 2008. Telomeres and aging. *Physiol Rev.* 88(2):557–579.
- Bairoch A, Apweiler R. 2000. The SWISS-PROT protein sequence database and its supplement TrEMBL in 2000. *Nucleic Acids Res.* 28(1):45–48.
- Bao W, Kojima KK, Kohany O. 2015. Repbase Update, a database of repetitive elements in eukaryotic genomes. *Mob DNA.* 6(1):11.
- Beddow JM, et al. 2015. Research investment implications of shifts in the global geography of wheat stripe rust. *Nat Plants.* 1(10):1–5.
- Bendtsen JD, Nielsen H, von Heijne G, Brunak S. 2004. Improved prediction of signal peptides: signalP 3.0. *J Mol Biol.* 340(4):783–795.
- Bernt M, et al. 2013. MITOS: improved de novo metazoan mitochondrial genome annotation. *Mol Phylogenet Evol.* 69(2):313–319.
- Boehm E. 1992. An ultrastructural pachytene karyotype for *Melampsora lini*. *Phytopathology* 82(10):1212.
- Boehm EWA, et al. 1992. An ultrastructural pachytene karyotype for *Puccinia graminis* f.sp. *tritici*. *Can J Bot.* 70(2):401–413.
- Buchfink B, Xie C, Huson DH. 2015. Fast and sensitive protein alignment using DIAMOND. *Nat Methods.* 12(1):59–60.

- Bueno-Sancho V, et al. 2017. Pathogenomic analysis of wheat yellow rust lineages detects seasonal variation and host specificity. *Genome Biol Evol.* 9(12):3282–3296.
- Cantu D, et al. 2011. Next generation sequencing provides rapid access to the genome of *Puccinia striiformis* f.sp. *tritici*, the causal agent of wheat stripe rust. *PLoS One* 6(8):e24230.
- Cantu D, et al. 2013. Genome analyses of the wheat yellow (stripe) rust pathogen *Puccinia striiformis* f.sp. *tritici* reveal polymorphic and haustorial expressed secreted proteins as candidate effectors. *BMC Genomics* 14(1):270.
- Chen J, et al. 2017. Loss of *AvrSr50* by somatic exchange in stem rust leads to virulence for *Sr50* resistance in wheat. *Science* 358(6370):1607–1610.
- Chen W, Wellings C, Chen X, Kang Z, Liu T. 2014. Wheat stripe (yellow) rust caused by *Puccinia striiformis* f.sp. *tritici*. *Mol Plant Pathol.* 15(5):433–446.
- Chin C-S, et al. 2016. Phased diploid genome assembly with single-molecule real-time sequencing. *Nat Methods.* 13(12):1050–1054.
- Cuomo CA, et al. 2016. Comparative analysis highlights variable genome content of wheat rusts and divergence of the mating loci. *G3 (Bethesda)* 7:361–376.
- Dale RK, Pedersen BS, Quinlan AR. 2011. Pybedtools: a flexible Python library for manipulating genomic datasets and annotations. *Bioinformatics* 27(24):3423–3424.
- Dobon A, Bunting DCE, Cabrera-Quio LE, Uauy C, Saunders D. 2016. The host-pathogen interaction between wheat and yellow rust induces temporally coordinated waves of gene expression. *BMC Genomics* 17(1):380.
- Duan X, et al. 2010. *Puccinia striiformis* f.sp. *tritici* presents high diversity and recombination in the over-summering zone of Gansu, China. *Mycologia* 102(1):44–53.
- Duplessis S, et al. 2011. Obligate biotrophy features unraveled by the genomic analysis of rust fungi. *Proc Natl Acad Sci U S A.* 108(22):9166–9171.
- Edgar RC. 2004. MUSCLE: multiple sequence alignment with high accuracy and high throughput. *Nucleic Acids Res.* 32(5):1792–1797.
- Ellis JG, Lagudah ES, Spielmeier W, Dodds PN. 2014. The past, present and future of breeding rust resistant wheat. *Front Plant Sci.* 5:641.
- Emms DM, Kelly S. 2019. OrthoFinder2: fast and accurate phylogenomic orthology analysis from gene sequences. *Genome Biol.* 20:238.
- Fletcher K, et al. 2019. Genomic signatures of heterokaryosis in the oomycete pathogen *Bremia lactucae*. *Nat Commun.* 10(1):2645.
- Flutre T, Duprat E, Feuillet C, Quesneville H. 2011. Considering transposable element diversification in de novo annotation approaches. *PLoS One* 6(1):e16526.
- Fouché S, et al. 2020. Stress-driven transposable element de-repression dynamics and virulence evolution in a fungal pathogen. *Mol Biol Evol.* 37(1):221–239.
- Frantzeskakis L, et al. 2018. Signatures of host specialization and a recent transposable element burst in the dynamic one-speed genome of the fungal barley powdery mildew pathogen. *BMC Genomics* 19(1):381.
- Frantzeskakis L, Kusch S, Panstruga R. 2019. The need for speed: compartmentalized genome evolution in filamentous phytopathogens. *Mol Plant Pathol.* 20(1):3–7.
- Frantzeskakis L, Németh MZ, et al. 2019. The *Parauncinula polyspora* draft genome provides insights into patterns of gene erosion and genome expansion in powdery mildew fungi. *mBio* 10(5):e01692–19.
- Garrison E, Marth G. 2012. Haplotype-based variant detection from short-read sequencing. *arXiv. 1207.3907 [q-bio]* [accessed 2017 Sep 15]. Available from: <http://arxiv.org/abs/1207.3907>.
- Gladioux P, et al. 2014. Fungal evolutionary genomics provides insight into the mechanisms of adaptive divergence in eukaryotes. *Mol Ecol.* 23(4):753–773.
- Grabherr MG, et al. 2011. Trinity: reconstructing a full-length transcriptome without a genome from RNA-Seq data. *Nat Biotechnol.* 29(7):644–652.
- Grandaubert J, Dutheil JY, Stukenbrock EH. 2019. The genomic determinants of adaptive evolution in a fungal pathogen. *Evol Lett.* 3(3):299–312.
- Grigoriev IV, et al. 2014. MycoCosm portal: gearing up for 1000 fungal genomes. *Nucleic Acids Res.* 42(D1):D699–D704.
- Haas BJ, et al. 2008. Automated eukaryotic gene structure annotation using EvidenceModeler and the program to assemble spliced alignments. *Genome Biol.* 9(1):R7.
- Heitman J. 2015. Evolution of sexual reproduction: a view from the fungal kingdom supports an evolutionary epoch with sex before sexes. *Fungal Biol Rev.* 29(3-4):108–117.
- Hoff KJ, Lange S, Lomsadze A, Borodovsky M, Stanke M. 2016. BRAKER1: unsupervised RNA-Seq-based genome annotation with GeneMark-ET and AUGUSTUS. *Bioinformatics* 32(5):767–769.
- Hovmøller MS, et al. 2016. Replacement of the European wheat yellow rust population by new races from the centre of diversity in the near-Himalayan region. *Plant Pathol.* 65(3):402–411.
- Hovmøller MS, Justesen AF. 2007. Rates of evolution of avirulence phenotypes and DNA markers in a northwest European population of *Puccinia striiformis* f.sp. *tritici*. *Mol Ecol.* 16(21):4637–4647.
- Hovmøller MS, Justesen AF, Brown J. 2002. Clonality and long-distance migration of *Puccinia striiformis* f.sp. *tritici* in north-west. Europe. *Plant Pathol.* 51(1):24–32.
- Hovmøller MS, Yahyaoui AH, Milus EA, Justesen AF. 2008. Rapid global spread of two aggressive strains of a wheat rust fungus. *Mol Ecol.* 17(17):3818–3826.
- Hubbard A, et al. 2015. Field pathogenomics reveals the emergence of a diverse wheat yellow rust population. *Genome Biol.* 16(1):23.
- Huerta-Cepas J, et al. 2016. eggNOG 4.5: a hierarchical orthology framework with improved functional annotations for eukaryotic, prokaryotic and viral sequences. *Nucleic Acids Res.* 44(D1):D286–D293.
- Hunt M, et al. 2015. Circlator: automated circularization of genome assemblies using long sequencing reads. *Genome Biol.* 16(1):294.
- Jin Y, Szabo LJ, Carson M. 2010. Century-old mystery of *Puccinia striiformis* life history solved with the identification of *Berberis* as an alternate host. *Phytopathology* 100(5):432–435.
- Jones P, et al. 2014. InterProScan 5: genome-scale protein function classification. *Bioinformatics* 30(9):1236–1240.
- Kim D, Langmead B, Salzberg SL. 2015. HISAT: a fast spliced aligner with low memory requirements. *Nat Methods.* 12(4):357–360.
- Koren S, et al. 2017. Canu: scalable and accurate long-read assembly via adaptive k-mer weighting and repeat separation. *Genome Res.* 27(5):722–736.
- Korovesi AG, Ntertilis M, Kouvelis VN. 2018. Mt-rps3 is an ancient gene which provides insight into the evolution of fungal mitochondrial genomes. *Mol Phylogenet Evol.* 127:74–86.
- Kozul R, et al. 2003. The complete mitochondrial genome sequence of the pathogenic yeast *Candida (Torulopsis) glabrata*. *FEBS Lett.* 534(1–3):39–48.
- Krumsiek J, Arnold R, Rattei T. 2007. Gepard: a rapid and sensitive tool for creating dotplots on genome scale. *Bioinformatics* 23(8):1026–1028.
- Kurtz S, et al. 2004. Versatile and open software for comparing large genomes. *Genome Biol.* 5(2):R12.
- Lang BF, Laforest M-J, Burger G. 2007. Mitochondrial introns: a critical view. *Trends Genet.* 23(3):119–125.
- Laslett D, Canback B. 2004. ARAGORN, a program to detect tRNA genes and tmRNA genes in nucleotide sequences. *Nucleic Acids Res.* 32(1):11–16.
- Lechner M, et al. 2011. Proteinortho: detection of (co-)orthologs in large-scale analysis. *BMC Bioinformatics* 12(1):124.

- Lei Y, et al. 2016. Virulence and molecular characterization of experimental isolates of the stripe rust pathogen (*Puccinia striiformis*) indicate somatic recombination. *Phytopathology* 107(3):329–344.
- Li C, et al. 2020. The complete mitochondrial genomes of *Puccinia striiformis* f.sp. *tritici* and *Puccinia recondita* f.sp. *tritici*. *Mitochondrial DNA B*. 5(1):29–30.
- Li F, Upadhyaya NM, et al. 2019. Emergence of the Ug99 lineage of the wheat stem rust pathogen through somatic hybridisation. *Nat Commun*. 10(1):15.
- Li H. 2013. Aligning sequence reads, clone sequences and assembly contigs with BWA-MEM. arXiv. 1303.3997 [q-bio] [accessed 2017 Sep 14]. Available from: <http://arxiv.org/abs/1303.3997>.
- Li Y, Xia C, Wang M, Yin C, Chen X. 2019. Genome sequence resource of a *Puccinia striiformis* isolate infecting wheatgrass. *Phytopathology* 109(9):1509–1512.
- Liu H, et al. 2018. Tetrad analysis in plants and fungi finds large differences in gene conversion rates but no GC bias. *Nat Ecol Evol*. 2(1):164–173.
- Lorrain C, et al. 2019. Advances in understanding obligate biotrophy in rust fungi. *New Phytol*. 222(3):1190–1206.
- Losada L, et al. 2014. Mobile elements and mitochondrial genome expansion in the soil fungus and potato pathogen *Rhizoctonia solani* AG-3. *FEMS Microbiol Lett*. 352(2):165–173.
- Lowe TM, Eddy SR. 1997. tRNAscan-SE: a program for improved detection of transfer RNA genes in genomic sequence. *Nucleic Acids Res*. 25(5):955–964.
- Marçais G, Kingsford C. 2011. A fast, lock-free approach for efficient parallel counting of occurrences of k-mers. *Bioinformatics* 27(6):764–770.
- Markell SG, Milus EA. 2008. Emergence of a novel population of *Puccinia striiformis* f.sp. *tritici* in eastern United States. *Phytopathology* 98(6):632–639.
- Maumus F, Quesneville H. 2014. Ancestral repeats have shaped epigenome and genome composition for millions of years in *Arabidopsis thaliana*. *Nat Commun*. 5(1):4104.
- Mboup M, et al. 2012. Genetic structure and local adaptation of European wheat yellow rust populations: the role of temperature-specific adaptation. *Evol Appl*. 5(4):341–352.
- McKinney W. 2010. Data structures for statistical computing in python. p. 51–56 [accessed 2017 Sep 15]. Available from: <http://conference.scipy.org/proceedings/scipy2010/mckinney.html>.
- Menardo F, et al. 2016. Hybridization of powdery mildew strains gives rise to pathogens on novel agricultural crop species. *Nat Genet*. 48(2):201–205.
- Miller ME, et al. 2018. De novo assembly and phasing of dikaryotic genomes from two isolates of *Puccinia coronata* f.sp. *avenae*, the causal agent of oat crown rust. *mBio* 9(1):e01650–e01717.
- Müller MC, et al. 2019. A chromosome-scale genome assembly reveals a highly dynamic effector repertoire of wheat powdery mildew. *New Phytol*. 221(4):2176–2189.
- Nattestad M, Schatz MC. 2016. Assemblytics: a web analytics tool for the detection of variants from an assembly. *Bioinformatics* 32(19):3021–3023.
- Nersisyan L, Arakelyan A. 2015. Computel: computation of mean telomere length from whole-genome next-generation sequencing data. *PLoS One* 10(4):e0125201.
- Park RF, Wellings CR. 2012. Somatic hybridization in the Uredinales. *Annu Rev Phytopathol*. 50(1):219–239.
- Pertea M, et al. 2015. StringTie enables improved reconstruction of a transcriptome from RNA-seq reads. *Nat Biotechnol*. 33(3):290–295.
- Petersen TN, Brunak S, von Heijne G, Nielsen H. 2011. SignalP 4.0: discriminating signal peptides from transmembrane regions. *Nat Methods*. 8(10):785–786.
- Quesneville H, et al. 2005. Combined evidence annotation of transposable elements in genome sequences. *PLoS Comp Biol*. 1(2):e22.
- Quinlan AR, Hall IM. 2010. BEDTools: a flexible suite of utilities for comparing genomic features. *Bioinformatics* 26(6):841–842.
- Radhakrishnan GV, et al. 2019. MARPLE, a point-of-care, strain-level disease diagnostics and surveillance tool for complex fungal pathogens. *BMC Biol*. 17(1):65.
- Ranallo-Benavidez TR, Jaron KS, Schatz MC. 2020. GenomeScope 2.0 and Smudgeplots: reference-free profiling of polyploid genomes. *Nat Commun*. 11:1432.
- Rapilly F. 1979. Yellow rust epidemiology. *Annu Rev Phytopathol*. 17(1):59–73.
- Rawlings ND, Barrett AJ, Finn R. 2016. Twenty years of the MEROPS database of proteolytic enzymes, their substrates and inhibitors. *Nucleic Acids Res*. 44(D1):D343–D350.
- Rodriguez-Algaba J, Walter S, Sørensen CK, Hovmøller MS, Justesen AF. 2014. Sexual structures and recombination of the wheat rust fungus *Puccinia striiformis* on *Berberis vulgaris*. *Fungal Genet Biol*. 70:77–85.
- rtg-tools. 2017. rtg-tools: RTG tools utilities for accurate VCF comparison and manipulation. *Real Time Genomics* [accessed 2017 Sep 15]. Available from: <https://github.com/RealTimeGenomics/rtg-tools>.
- Salcedo A, et al. 2017. Variation in the AvrSr35 gene determines Sr35 resistance against wheat stem rust race Ug99. *Science* 358(6370):1604–1606.
- Savary S, et al. 2019. The global burden of pathogens and pests on major food crops. *Nat Ecol Evol*. 3(3):430–439.
- Schwessinger B. 2017. Fundamental wheat stripe rust research in the 21(st) century. *New Phytol*. 213(4):1625–1631.
- Schwessinger B, et al. 2018. A near-complete haplotype-phased genome of the dikaryotic wheat stripe rust fungus *Puccinia striiformis* f.sp. *tritici* reveals high interhaplotype diversity. *mBio* 9(1):e02275–e02317.
- Schwessinger B, Rathjen JP. 2017. Wheat Rust Diseases Extraction of high molecular weight DNA from fungal rust spores for long read sequencing. In: *Methods in molecular biology*. New York: Humana Press. p. 49–57.
- Seudre O, et al. 2018. Why outcross? The abandon-ship hypothesis in a facultative outcrossing/selfing fungal species. *Fungal Genet Biol*. 120:1–8.
- Shirleen Roeder G. 1983. Unequal crossing-over between yeast transposable elements. *Mol Gen Genet*. 190(1):117–121.
- Simão FA, Waterhouse RM, Ioannidis P, Kriventseva EV, Zdobnov EM. 2015. BUSCO: assessing genome assembly and annotation completeness with single-copy orthologs. *Bioinformatics* 31(19):3210–3212.
- Singh RP, et al. 2016. Disease impact on wheat yield potential and prospects of genetic control. *Annu Rev Phytopathol*. 54(1):303–322.
- Sørensen CK, Hovmøller MS, Leconte M, Dedyrer F, de Vallavieille-Pope C. 2014. New races of *Puccinia striiformis* found in Europe reveal race specificity of long-term effective adult plant resistance in wheat. *Phytopathology* 104(10):1042–1051.
- Sørensen CK, Thach T, Hovmøller MS. 2016. Evaluation of spray and point inoculation methods for the phenotyping of *Puccinia striiformis* on wheat. *Plant Dis*. 100(6):1064–1070.
- Sperschneider J, Dodds PN, Gardiner DM, Singh KB, Taylor JM. 2018. Improved prediction of fungal effector proteins from secretomes with EffectorP 2.0. *Mol Plant Pathol*. 19(9):2094–2110.
- Sperschneider J, et al. 2016. EffectorP: predicting fungal effector proteins from secretomes using machine learning. *New Phytol*. 210(2):743–761.
- Sperschneider J, et al. 2020. The stem rust fungus *Puccinia graminis* f.sp. *tritici* induces waves of small RNAs with opposing profiles during wheat infection. *bioRxiv*. 469338. doi:10.1101/469338.
- Stam R, et al. 2018. A new reference genome shows the one-speed genome structure of the barley pathogen *Ramularia collo-cygni*. *Genome Biol Evol*. 10(12):3243–3249.
- Steele KA, Humphreys E, Wellings CR, Dickinson MJ. 2001. Support for a stepwise mutation model for pathogen evolution in Australasian

- Puccinia striiformis* f.sp. *tritici* by use of molecular markers. *Plant Pathol.* 50(2):174–180.
- Stone CL, Buitrago MLP, Boore JL, Frederick RD. 2010. Analysis of the complete mitochondrial genome sequences of the soybean rust pathogens *Phakopsora pachyrhizi* and *P. meibomia*. *Mycologia* 102(4):887–897.
- Stukenbrock EH. 2016. The role of hybridization in the evolution and emergence of new fungal plant pathogens. *Phytopathology* 106(2):104–112.
- Suyama M, Torrents D, Bork P. 2006. PAL2NAL: robust conversion of protein sequence alignments into the corresponding codon alignments. *Nucleic Acids Res.* 34(Web Server):W609–W612.
- Taylor JW, Hann-Soden C, Branco S, Sylvain I, Ellison CE. 2015. Clonal reproduction in fungi. *Proc Natl Acad Sci U S A.* 112(29):8901–8908.
- Testa AC, Hane JK, Ellwood SR, Oliver RP. 2015. CodingQuarry: highly accurate hidden Markov model gene prediction in fungal genomes using RNA-seq transcripts. *BMC Genomics* 16(1):170.
- Thach T, Ali S, de Vallaville-Pope C, Justesen AF, Hovmøller MS. 2016. Worldwide population structure of the wheat rust fungus *Puccinia striiformis* in the past. *Fungal Genet Biol.* 87:1–8.
- Thach T, et al. 2015. Recovery and virulence phenotyping of the historic ‘Stubbs collection’ of the yellow rust fungus *Puccinia striiformis* from wheat. *Ann Appl Biol.* 167(3):314–326.
- Tillich M, et al. 2017. GeSeq – versatile and accurate annotation of organellar genomes. *Nucleic Acids Res.* 45(W1):W6–W11.
- Torriani SFF, et al. 2014. Comparative analysis of mitochondrial genomes from closely related *Rhynchosporium* species reveals extensive intron invasion. *Fungal Genet Biol.* 62:34–42.
- Underwood CJ, Choi K. 2019. Heterogeneous transposable elements as silencers, enhancers and targets of meiotic recombination. *Chromosoma* 128(3):279–296.
- vcflib. 2017. vcflib: a simple C++ library for parsing and manipulating VCF files, + many command-line utilities. vcflib [accessed 2017 Sep 15]. Available from: <https://github.com/vcflib/vcflib>.
- Walker BJ, et al. 2014. Pilon: an integrated tool for comprehensive microbial variant detection and genome assembly improvement. *PLoS One* 9(11):e112963.
- Walter S, et al. 2016. Molecular markers for tracking the origin and worldwide distribution of invasive strains of *Puccinia striiformis*. *Ecol Evol.* 6(9):2790–2804.
- Wang N, et al. 2014. Novel telomere-anchored PCR approach for studying sexual stage telomeres in *Aspergillus nidulans*. *PLoS One* 9(6):e99491.
- Wang Y, et al. 2012. MCScanX: a toolkit for detection and evolutionary analysis of gene synteny and collinearity. *Nucleic Acids Res.* 40(7):e49.
- Weir W, et al. 2016. Population genomics reveals the origin and asexual evolution of human infective trypanosomes. *eLife Sci.* 5:e11473.
- Wellings CR. 2007. *Puccinia striiformis* in Australia: a review of the incursion, evolution, and adaptation of stripe rust in the period 1979–2006. *Aust J Agric Res.* 58(6):567–575.
- Wellings CR. 2011. Global status of stripe rust: a review of historical and current threats. *Euphytica* 179(1):129–141.
- Wellings CR, McIntosh RA. 1990. *Puccinia striiformis* f.sp. *tritici* in Australasia: pathogenic changes during the first 10 years. *Plant Pathol.* 39(2):316–325.
- Xia C, et al. 2018. Genomic insights into host adaptation between the wheat stripe rust pathogen (*Puccinia striiformis* f.sp. *tritici*) and the barley stripe rust pathogen (*Puccinia striiformis* f.sp. *hordei*). *BMC Genomics* 19(1):664.
- Yang Z, Nielsen R. 2000. Estimating synonymous and nonsynonymous substitution rates under realistic evolutionary models. *Mol Biol Evol.* 17(1):32–43.
- Yin Y, et al. 2012. dbCAN: a web resource for automated carbohydrate-active enzyme annotation. *Nucleic Acids Res.* 40(W1):W445–W451.
- Zeyl C. 2009. The role of sex in fungal evolution. *Curr Opin Microbiol.* 12(6):592–598.
- Zhao T, Schranz ME. 2019. Network-based microsynteny analysis identifies major differences and genomic outliers in mammalian and angiosperm genomes. *Proc Natl Acad Sci U S A.* 116:2165–2174.
- Zheng W, et al. 2013. High genome heterozygosity and endemic genetic recombination in the wheat stripe rust fungus. *Nat Commun.* 4(1):2673.

Associate editor: Jason Stajich